

The High Throughput X-ray Spectroscopy (HTXS) Mission

The Technology Roadmap

A report to NASA prepared by

The HTXS Mission Study Team

California Institute of Technology
Columbia University
Goddard Space Flight Center
Marshall Space Flight Center
Massachusetts Institute of Technology
Naval Research Laboratory
Osservatorio Astronomico di Brera
Penn State University
Smithsonian Astrophysical Observatory
University of Arizona
University of Colorado
University of Maryland
University of Michigan
University of Washington
University of Wisconsin

Contents

| | | |
|----------|---|-----------|
| 1 | Introduction | 1 |
| 1.1 | The HTXS Mission | 1 |
| 2 | The Spectroscopy X-ray Telescope (SXT) Optics | 2 |
| 2.1 | Introduction | 2 |
| 2.2 | Current Status | 2 |
| 2.3 | Success Criteria | 2 |
| 2.4 | Replicated Mirror Shells | 3 |
| 2.4.1 | Technology Requirement | 3 |
| 2.4.2 | Metrics | 3 |
| 2.5 | Segmented Mirrors | 6 |
| 2.5.1 | Technology Requirement | 6 |
| 2.5.2 | Metrics | 7 |
| 2.5.3 | Achieving required angular resolution | 7 |
| 2.5.4 | Large diameter conical mirrors | 8 |
| 2.6 | Figured foils | 9 |
| 2.7 | Milestones for the Mirror Development | 10 |
| 2.8 | Existing Funding | 12 |
| 2.8.1 | Replicated Mirror Shells | 12 |
| 2.8.2 | Segmented Foil Mirrors | 12 |
| 3 | X-Ray Calorimeters | 13 |
| 3.1 | Introduction | 13 |
| 3.2 | Present Status of X-Ray Microcalorimeters | 14 |
| 3.3 | Limitations of Microcalorimeters with Semiconducting Thermometers | 15 |
| 3.4 | Absorbers for Semiconductor Thermometer Calorimeters | 16 |
| 3.5 | New Technologies for Semiconductor Thermometers | 17 |
| 3.6 | Superconducting Transition Edge Thermometers | 18 |
| 3.7 | Larger Arrays of Microcalorimeters | 18 |
| 3.8 | The Path Toward Higher Spectral Resolution | 19 |
| 3.9 | References | 19 |
| 3.10 | Metrics | 20 |
| 3.11 | Mission Criticality | 20 |

| | | |
|----------|--|-----------|
| 3.12 | Milestones for Calorimeter Development | 21 |
| 4 | The Reflection Grating Array | 22 |
| 4.1 | Introduction | 22 |
| 4.2 | Current Status | 22 |
| 4.3 | Technology Requirements | 23 |
| 4.3.1 | Mass Reduction | 23 |
| 4.3.2 | Improved Scientific Performance | 24 |
| 4.4 | Metrics | 24 |
| 4.5 | Mission Criticality | 24 |
| 4.6 | Milestones for Grating Development | 25 |
| 5 | CCDs | 26 |
| 5.1 | Introduction | 26 |
| 5.2 | Metrics | 27 |
| 5.3 | Mission Criticality | 28 |
| 5.4 | Milestones for CCD Development | 29 |
| 6 | The Cryogenics Subsystems | 30 |
| 6.0.1 | Technology Requirement | 30 |
| 6.1 | The Possible Options | 30 |
| 6.2 | Success Criteria | 31 |
| 6.3 | Option 1: Cryocooler, stored liquid helium and sub-Kelvin cooler | 32 |
| 6.3.1 | Metrics for the Baseline Cooling System | 33 |
| 6.3.2 | Mechanical coolers | 34 |
| 6.3.3 | Adiabatic Demagnetization Refrigerator | 34 |
| 6.4 | Hybrid Cooling System 2: A Two Stage Mechanical Cooler Design | 34 |
| 6.4.1 | Technology Requirement | 34 |
| 6.4.2 | Metrics for Baseline Hybrid Cryogenic Cooling System 2 | 36 |
| 6.4.3 | Mechanical cooler | 36 |
| 6.4.4 | Adiabatic Demagnetization Refrigerator | 36 |
| 6.5 | Mission criticality | 36 |
| 6.6 | Milestones for the Cryocooler Development | 37 |
| 7 | Hard X-ray telescope (HXT) | 39 |

| | | |
|----------|---|-----------|
| 7.1 | Requirements for the HXT | 39 |
| 7.2 | Background: Technical Approach to Hard X-ray Focusing | 40 |
| 7.3 | Example Telescope Designs | 40 |
| 7.3.1 | Graded Multilayer Telescope Design | 41 |
| 7.3.2 | Low Graze Angle Telescope | 46 |
| 7.4 | Technology Status and Development Requirements | 47 |
| 7.4.1 | Hard X-ray Optics | 47 |
| 7.4.2 | HXT Detectors | 49 |
| 7.4.3 | Milestones for the HXT Development | 51 |
| 8 | Extendible Optical Bench (EOB) | 52 |
| 8.1 | Introduction | 52 |
| 8.2 | Current Status | 52 |
| 8.3 | Success Criteria | 52 |
| 8.4 | Technology Requirements | 53 |
| 8.5 | Metrics | 53 |
| 8.6 | Mission Criticality | 53 |
| 8.7 | Deployable Structures | 53 |
| 8.7.1 | Telescoping Tubes | 53 |
| 8.8 | Deployable Booms | 54 |
| 8.9 | Other Concepts | 54 |
| 8.10 | Precision Remote Control Alignment Systems | 54 |
| 8.11 | Thermal Control | 54 |
| 8.12 | Deployable signal and power cables | 55 |
| 8.13 | Deployable Scattered Light Shield | 55 |
| 8.14 | Milestones for the EOB Development | 56 |
| 9 | Mission Study | 57 |
| 9.1 | Study Areas | 57 |
| 9.1.1 | Science Working Group and Science Study Team | 57 |
| 9.1.2 | Reports | 57 |
| 9.1.3 | Technical Interchange Meetings and Contractors Visits | 57 |
| 9.2 | Pre Phase-A mission studies | 58 |

1 Introduction

1.1 The HTXS Mission

The fundamental science questions to be addressed by HTXS require very substantial increases in effective area, energy resolution, and energy bandpass. To accomplish these ambitious increases at an affordable mission cost, we must introduce new approaches for the development and operation of the HTXS mission and take advantage of technical advances as well. The primary goal of the HTXS Roadmap document is to outline a strategy for achieving the currently stated scientific objectives at a minimum of cost and technical risk. An essential feature of this concept involves minimization of cost (\sim \$350M for development and \sim \$500–600M including launches) and risk by building six identical modest satellites to achieve the large area.

Key technologies relating directly to the HTXS science instruments and spacecraft include: state-of-the-art X-ray mirrors, multilayer coatings, spectrometers, low-energy and hard X-ray detectors, cryogenic systems, extendible optical benches, lightweight satellite buses, and advanced communications systems. Development efforts in each of these areas will have utility for a variety of NASA programs including HTXS.

The specific HTXS mission requirements that drive the Technology Roadmap derive from its large effective area (\sim 15,000 cm² at 1 keV), high spectral resolution ($E/\Delta E \sim$ 300–3000), and broad energy bandpass (0.25–40 keV and possibly up to 100 keV). These requirements can be met by using replicated optics with reflection gratings, charge-coupled device detectors (CCDs), quantum micro-calorimeters, and cadmium zinc telluride (CZT), germanium, and/or xenon hard X-ray detectors.

The Technology Roadmap for HTXS points the way for the near-term development efforts that must be undertaken. For each of the technology development areas, we benchmark the current status of the field, identify key directions for technology investment, provide metrics to be utilized for the study, denote program milestones tied to the study timeline, call out achievable goals, and denote success criteria for each development and study effort. To ensure the success of these efforts, a well-balanced mix of university, government, and industry participation is essential.

Achieving these goals means approaching the study with an eye towards using moderately improved current and conventional technologies, as well as alternative, novel, and even revolutionary techniques. This two-pronged approach characterizes most of the areas we identify for technology investment. Careful selection of alternatives to pursue at an early point in the program, with decision points well-noted, enables the development of new technology at acceptable costs within the study timeline - and provides a path to achieve the HTXS capabilities at reduced power, weight, and mission cost.

2 The Spectroscopy X-ray Telescope (SXT) Optics

2.1 Introduction

Two approaches are being considered for the X-ray mirrors for the high-throughput spectrometer: 1) replica shells, as used on XMM, Jet-X, and SAX, and 2) segmented (foil) mirrors, as used on ASTRO-E (and derived from the ASCA and BBXRT programs). Both techniques show promise of satisfying the HTXS scientific requirements, and indeed, if an existing mirror possessed the better qualities of the two approaches, then no development would be necessary. However, neither approach currently meets all of the HTXS requirements, and a substantial technological investment is required either to improve the angular resolution of the segmented optics by a factor of 4, or reduce the weight of the replicated shells by a factor of ten.

2.2 Current Status

The state of the art in replicated shell mirrors is defined by the work of Oberto Citterio and his colleagues at Osservatorio Astronomico di Brera (OAB) in Milan, Italy. Their mirrors for the JET-X telescope have measured HPDs (half power diameters) slightly better than the HTXS target of 15 arc seconds at 0.27, 1.49, and 8.05 keV. However, the thicknesses of these shells would result in a total HTXS mirror mass of about 3,000 kg, compared with the current budget of about 250 kg. The technology development program described below is directed towards reducing this mass to the required value without an unacceptable sacrifice of performance.

The state of the art in segmented mirrors is defined by the work of Peter Serlemitsos and his colleagues at GSFC. A foil mirror of the size needed for the HTXS mission would be within the 250 kg mass budget, but the required spatial resolution has not yet been attained. The best HPD for a completed foil mirror assembly is about 3 arc minutes; these results were limited by ripple in the lacquer dipped foil with characteristic length scales of a few mm. The foils being prepared for the Astro-E mission, which are manufactured by a different process described below, have a HPD of 1 arc minute and 90% power diameters of ~ 3 arc minutes, and mirrors made from these foils should have performance comparable to that of the individual foils. To meet the spectroscopic goals of the HTXS mission, however, the HPD must be improved by a factor of 4 to meet the requirement of 15 arc seconds.

2.3 Success Criteria

The success criterion for both approaches to the mirror manufacture is to demonstrate the capability of constructing a 1-1.3 m diameter mirror with a half power diameter of no more than 15 arc seconds, and a total mass of no more than 250 kg.

2.4 Replicated Mirror Shells

2.4.1 Technology Requirement

The best existing replicated shell mirrors were made by taking an aluminum mandrel coated with electroless nickel (Kanigen), polishing the nickel to obtain an accurate figure and surface roughness, evaporating or sputtering about 1000 Å of gold onto the mandrel, electroplating with nickel to a thickness of order 1 mm, and removing the nickel from the mandrel at lower temperatures by differential thermal expansion. The gold layer sticks to the electroplated nickel and maintains the accurate figure and low surface roughness of the mandrel.

The electroplated nickel will have some internal residual stress, which will cause some deformation of the optical element; the dominant distortion is the low energy mode in which the mirror becomes oval at both ends, but with a 90 degree change in the azimuthal angle of the long oval axis. Citterio and his colleagues found the following empirical relationship for the required wall thickness t :

$$t = K \frac{R}{HPD_w^{1.37}}$$

where R is the radius of the mirror, HPD_w is the contribution of the wall stress induced distortions to the HPD in arc seconds, and K is a process and material dependent empirical constant which was 0.16 for their electroplated nickel. The wall thicknesses used to obtain the 3,000 kg estimate for an electroformed mirror were calculated using this formula.

2.4.2 Metrics

The purpose of the replicated shell mirror technology program is to demonstrate that a replica mirror can be constructed that meets the HTXS weight requirement without sacrificing the spatial resolution, which already is adequate for HTXS. Three approaches will be explored to reducing the mirror weight: more efficient use of the substrate material than a uniform thickness shell, reducing the internal stress in the shells, and introducing a different manufacturing process which would be characterized by a different functional dependence.

1. *Reducing internal stress.* The magnitude and even the sign of the internal stress in the electroless nickel is a function of the density of trace elements in the coating, and this density varies with the current density. Thus a stress free coating can be obtained if the current density is sufficiently uniform and well controlled. The MSFC group has developed virtually stress free shells by measuring the accumulated internal stress during the coating and adjusting the plating current to keep the total internal stress small. We will attempt to improve the uniformity of the plating current over the mandrel and between the mandrel and the stress monitoring sensor by a high fidelity simulation of the plating process and by careful adjustment of the plating geometry using a high fidelity simulation of the process. If necessary, we will use multiple plating anodes to produce the uniform, stress-free shells. We will use existing modeling codes, with modifications as appropriate. If successful, this will allow thinner nickel walls than have been required previously.

2. *Better use of material* Presently the deformation forces, which are proportional to the mirror volume, are counteracted by the same wall volume; this is successful because the internal force scales as the wall thickness whereas the stiffness against the dominant distortion scales as the cube of the thickness. It is reasonable to expect that the same performance can be achieved with a smaller mass if the same stiffness to internal force ratio is maintained, but with the internal forces reduced by thinning the walls and the stiffness augmented by separate structure. Two approaches will be investigated.

The OAB group will electroplate a thin nickel shell onto a mandrel, temporarily bond a stiff auxiliary support ring to the nickel while it is still on the mandrel, and hence undistorted, remove the shell and support ring from the mandrel, bond the shell to the final support structure, and remove the auxiliary support ring. This approach does not require the shell to maintain its own roundness at any time, and does not require an extremely precise support structure since the final bond between support structure and mirror shell can accommodate small variations in the gap between them.

The MSFC group has produced shells with the required small wall thicknesses which were supported against distortion by adding radial nickel rings (with a small axial extent) after the thin mirror walls are formed. The radial rings are attached by introducing them into the electroplating bath near the end of the process and forming an electroplated attachment between the thin mirror walls and the rings. The support rings are in their equilibrium shape before attachment and do not contribute to the forces causing the distortion. A mirror design in which the rings provide the stiffness required to counteract the mirror wall internal stresses found previously at OAB would have a mass of approximately 300 kg, and satisfy the HTXS requirements. The MSFC group produced these shells to develop the attachment process, and were successful, but no performance demonstration was achieved because an old and unsatisfactory mandrel was used. We will now try this technique with a better mandrel so that the expected performance can be evaluated. More thorough modelling of the mechanical properties of such assemblies also must be performed.

3. *Better choice of material.* If the substrate material were stiffer, less dense, and in equilibrium with its internal stresses at the time of attachment to the mandrel, then thinner walled substrates would be possible. The basic approach consists of separately forming the mirror supporting or substrate shells, bonding them to the gold coated mandrel, and removing the shell. The epoxy would accommodate small differences in the shapes of the mandrel and substrate, so the substrate need not be as precisely made as the polished mandrel. Three materials are being considered, chemical vapor deposited silicon carbide (CVD SiC), a plasma torch deposited aluminum oxide (with some titanium oxide) ceramic ($\text{Al}_2\text{O}_3/\text{TiO}$), and a carbon fiber reinforced cyanate ester (CFRP, the "P" standing for plastic). The ceramic (SiC or $\text{Al}_2\text{O}_3/\text{TiO}$) approach would assure a mechanically stable system, whereas the CFRP approach would be slightly lighter and less expensive. The expected distortion in this case is driven by the large scale roundness errors in the substrate; the epoxy bonding process will tend to distort the substrate towards the better shaped and stiffer mandrel, and the resulting shell will be distorted when removed from the mandrel.

The mandrels in $\text{Al}_2\text{O}_3/\text{TiO}$ process actually remain at room temperature in spite of the alarming sound of the plasma torch, which offers the possibility that the carrier could be formed directly on the optical mandrel, thereby simplifying the process,

eliminating the mandrels for the carrier, and avoiding the distortions introduced by the epoxy bonding process.

We presently assume that the Ceramic or CFRP walls would have to provide the same stiffness as the electroformed nickel walls of existing mirrors. We also have assumed that the large scale internal tolerances must be comparable with the desired large scale tolerances of the final mirror. These very conservative assumptions result in a mass of about 560 kg for the SiC (with about 13% local lightweighting) and 470 kg for the CFRP. However, the actual wall thicknesses required, although surely less than those based upon our present assumptions, are not known accurately. The optimum balance between mirror shell tolerances and wall thickness must be determined by the combination of an experimental program with different wall thicknesses and a more thorough mechanical modelling of the process. We also are investigating ribbed ceramic shells to allow thinner walls and further reduce the weights for these designs.

Previous attempts to use CFRP have suffered from dimensional instability resulting from water absorption/desorption and print through of the carbon fibers introducing high frequency surface errors. The cyanate ester is less sensitive to water absorption, and the shells can be nickel coated, which should both provide a seal and mitigate the carbon fiber print through problem. These expected improvements must, however, be demonstrated. It also may be useful to electroplate a very thin nickel buffer coating over the gold covered mandrel to improve the subsequent bonding with either the SiC or CFRP carrier; this also would reduce the carbon fiber print through problem in the CFRP case.

The dimensional accuracies of the CFRP mirror shells can be improved by forming them on a better mandrel; we plan to make multiple use of mandrels for this purpose. We will use a polished mandrel for thin electroformed replicas and the ceramic substrate mirror shells as discussed above. The mandrel then will be coated with a thin layer of gold as a release agent and a thin layer of electroformed nickel to provide a less fragile surface, and used as a master to form very accurately dimensioned CFRP shells. Subsequently, the mandrel will be reduced in radius by the desired bond thickness, repolished and coated with gold. The CFRP shells will be bonded to the now slightly smaller mandrel and separated (keeping the gold coating layer) to form a mirror as discussed above. The improved dimensional accuracies of the shells should reduce the distortion of the substrate towards the stiffer mandrel during the epoxy bonding process, and hence reduce the distortions which can occur when the shell is removed from the mandrel.

4. *Mandrel production and coatings.* Existing mandrel technology is adequate for the HTXS mission, but there would be economic advantages if adequate mandrels could be obtained using the diamond turning process to provide the desired figure and subsequent polishing to yield the desired low surface roughness. The MSFC group has produced mandrels which have the requisite low frequency errors, but also have somewhat excessive high frequency surface roughness which must be improved. Their polishing process also must be improved to either avoid degrading the figure of the diamond turned mandrel or to correct it; both low contact force computer controlled polishing, such as was used for AXAF, and ion polishing are being investigated for figure correction. The state of the art is such that a reasonable success criteria would be a five arc second half power diameter if mandrel figure correction is used, although

we do not expect this to be required for the 15 arc second half power diameters required for this program.

Mandrel durability also may be improved by coating the mandrel with a harder surface, such as titanium nitride, but the release and polishing properties of such surface coatings must be determined. We intend to coat the mirrors with iridium by internal sputtering, such as was done with the AXAF mirrors; the GSFC group has shown that this does not degrade the roughness of the gold separation layer. However, it would be economically advantageous to coat the iridium directly upon the mandrel, perhaps with a release agent, and avoid the subsequent sputtering. Approaches of this type will be investigated.

2.5 Segmented Mirrors

2.5.1 Technology Requirement

In a segmented conical mirror, the precisely curved surfaces that would theoretically yield a perfect image on axis have been replaced by simple cones. This offers a number of advantages: reduced weight and increased aperture utilization (thick-walled substrates are replaced by thin foils), and simpler manufacture (i.e., lower cost). Additionally, it becomes advantageous to manufacture mirrors in angular segments (traditionally quadrants) instead of full surfaces of revolution (hence the term “segmented”). What is sacrificed in using the so-called “conical approximation” is the potential for a perfect image. Instead, the actual image quality depends on the projected width of the foil reflectors on the focal plane, which in turn is a function of the length of the reflectors and the average grazing angle. If the reflector length and mirror diameter are held constant, then the intrinsic image size improves as the focal length is increased. For instance, an 8 m focal length mirror with a 1 m diameter and 10 cm reflectors (the size used for Astro-E) has an intrinsic image half power diameter of 13 arc seconds; increasing the focal length to 15 m reduces the HPD to 4 arc seconds. On the other hand, for a given focal length and diameter, reducing the length of the reflectors yields a proportional decrease in intrinsic resolution, but at the expense of complexity (an increased number of reflectors) and collecting area. An 8 m focal length mirror with a 1 m diameter and 5 cm reflectors has a 6.5 arc second HPD. In order to meet the spatial resolution requirement for HTXS using a conical mirror, an image quality approaching the theoretical limit must be attained. The theoretical resolution can be improved, thus providing less stringent fabrication tolerances, either by a careful choice of design parameters, or by using reflecting elements whose surfaces more closely resemble those of a Wolter I mirror than the currently used cones.

A typical mirror is populated by 100 or more foil reflector pairs. The current method of foil reflector production consists of replicating the surface of a drawn Pyrex mandrel. The mandrels, which are carefully selected lengths of Pyrex tubing used for commercial purposes, have inherently smooth surfaces on a microscopic scale (less than 1 mm), but may have large local slope errors. The first step is the selection of a mandrel by measuring the local axial slope errors and roundness. This is followed by sputtering about 2,000 Angstrom of gold onto the mandrel. The aluminum foil substrate (typically 125 microns thick) is cut to the correct axial length and shaped into a segment of a cone by heat treating the foil while it is in contact with a forming mandrel. The formed foil and gold covered glass mandrel are

both sprayed with a thin layer of epoxy under computer control, brought into contact in a vacuum, and placed into an oven to allow the epoxy to cure at an elevated temperature. The foil is matched to a desired diameter in the assembly, cut to the proper azimuthal length, and inserted into a precisely machined housing, in which it is supported by alignment bars located azimuthally every few degrees. These alignment bars can be adjusted radially to optimize the performance of the foils as a group.

The geometric or diffraction limits to the mirror performance are sufficient to meet the requirements for the HTXS program. The quality of the microscopic surface is dictated by the smoothness of the glass mandrel, and is currently 3 Angstrom rms, which means that X-rays will reflect specularly (without significant scatter) off the reflector surfaces throughout the energy range of the mirror. The present performance appears to be limited by a combination of three factors: figure errors in the glass mandrels, the accuracy with which the foil substrates hold the desired shape, and the accuracy to which the alignment bars locate the reflecting surfaces.

Also, the largest diameter conical mirror that has been constructed at GSFC for spaceflight use has a diameter of 40 cm, and a focal length of 4.5 m, both of which are considerably smaller than the projected HTXS dimensions.

2.5.2 Metrics

In order to meet the HTXS requirements, there are two primary milestones that segmented mirrors must meet: 1) The required angular resolution must be attained, which in turn requires improvements in reflector surfaces and fixturing accuracy. 2) The ability to fabricate one meter class mirrors must be demonstrated. Associated with each of these are decision points regarding design and fabrication details, as documented below.

2.5.3 Achieving required angular resolution

In order to approach the intrinsic angular resolution of conical mirrors, two sources of blurring must be significantly reduced: surface irregularities on the millimeter to centimeter scale, and imprecise fixturing of the reflectors. If improvement in spatial resolution beyond this is required, then curvature must be introduced onto the reflector surface during replication, so that it more closely approximates the ideal reflection surface.

1. *Choice of mandrel.* Mandrels that yield microscopically smooth and macroscopically accurate replicated surfaces are the key to the success of foil mirrors. Production of these might be the most expensive item associated with the high throughput mirror, so selection of the most cost effective approach is essential. The current mandrels, used for Astro-E, are carefully selected sections of commercial grade, drawn Pyrex pipe, with no additional polishing. It is possible that application of more stringent selection criteria to the Pyrex pipe can yield a set of mandrels meeting the HTXS requirements. Even if this is the case, it does not entirely resolve the mandrel choice issue: the drawn Pyrex is available in diameters no larger than ~ 50 cm, so at least the larger diameter mandrels must be fabricated differently. We will pursue the following four approaches regarding mandrels, and select the best one or combination on the basis of resulting angular resolution vs. cost:

- more careful selection of commercial glass;
- custom manufactured drawn Pyrex tubing;
- figured and polished quartz or Zerodur mandrels; and
- metal mandrels (superpolished electroless Ni on diamond turned Al).

Selection of mandrel manufacturing approach must be made by the end of FY 1999.

2. *Fixturing accuracy.* The reflectors in a conical mirror are held in place radially by grooves cut into a set of thin alignment bars at the entrance and exit of each housing. The current alignment bars, fabricated using electronic discharge machining, locate reflectors with an average accuracy of 10 microns or better. The current design must allow sufficient clearance within the grooves to allow the reflectors to be slid into place without binding and not introduce high spatial frequency ripples on the reflecting surfaces. To achieve the fixturing accuracy required for the HTXS (less than 5 microns on average), a more accurate approach to alignment bar manufacture, potentially resulting in a new approach to mirror assembly, must be introduced. We will investigate several approaches: more precise electronic discharge machining, use of diamond turning as the final machining step, and micro lithography. One promising new micro lithographic approach we will investigate is “deep plasma etching,” a technique pioneered by our collaborators at MIT, by which structures can be etched to a depth of hundreds of microns. Fixtures both meeting the accuracy requirement and capable of holding meter diameter foils must be developed and demonstrated by the end of FY 1999.

Utilization of accurate alignment bars to improve spatial resolution will have implications for the reflector manufacture. The current oversized alignment bar slots allow not only for straightforward mirror assembly, but for variations in reflector thickness as well. Thus we must develop controls within the reflector manufacture process that ensure uniform reflector thickness to 1 micron. Additionally, it is unclear whether the current assembly technique, sliding the foil radially through the alignment bar slots in an assembled fixture, can be used when the clearances have been reduced. We will investigate alternative approaches to mirror assembly

2.5.4 Large diameter conical mirrors

If a meter-class mirror is to be developed over the next several years, a prototype must be demonstrated as early in the program as possible. First we must determine the degree to which our current mirror and housing fabrication techniques can be scaled to larger sizes. We will procure a series of ~ 1 m diameter mandrels, and replicate large diameter foil reflector segments. Simultaneously we will fabricate a prototype housing based on our 40 cm diameter units. X-ray and optical performance tests of a mirror unit will enable us to decide whether a different reflector or housing fabrication approach is necessary. This must be accomplished by the end of FY 1998.

Our goal is to have a full sized prototype mirror segment that meets the performance requirements by the end of FY 2000.

2.6 Figured foils

The theoretical performance of the segmented mirrors can be improved by using a closer approximation to the desired surfaces than the present cones. We are investigating two approaches for this purpose.

We will replicate a properly curved mandrel using techniques similar to those now employed with the cylindrical mandrels. The required sagittal depth of the desired surfaces is much less than the thickness of the epoxy layer which currently exists between mandrel and foil, and we may find that the relaxed shape of the foils thus produced will retain enough of the curvature introduced by the mandrel to meet our requirements. Preliminary tests at GSFC indicate that it is indeed possible to replicate an axially curved surface onto a conical foil substrate without loss of fidelity. If necessary, the computer controlled application of the epoxy will be adjusted to better accommodate the figure mismatch between the foils and the desired optical surface.

Mark Schattenburg of MIT has suggested an alternate approach in which ion figured silicon wafers or sheets are bent to the desired shape. The sheets would be supported at relatively few locations, where their azimuthal slopes also would be controlled. A simple flat, constant thickness sheet deformed in this manner will not yield the desired optical surface. However, the approximation by selectively varying the thickness of the sheet. Initial computer models of this process, in which the boundary conditions and material removal are iterated towards an optimum shape, are quite promising, the rms values of the residual mechanical errors being about one third of the thickness of the sheet, which would permit essentially perfect surfaces to be formed. This would avoid errors caused by the mandrel imperfections or by plastic deformation of the aluminum foils, and it is reasonable to expect a few arc second resolution. The ion polished silicon wafers are known to be very smooth, so good scattering properties also should be obtained.

2.7 Milestones for the Mirror Development

One of the most critical decisions regarding HTXS instrumentation is the choice of mirror design. In order to allow the maximum of time for both designs to mature, this decision should be made as late as possible without introducing delays into the overall mission schedule. Thus this decision should be reached at the end of the technology development phase, at the end of FY2000. Prior to then, an aggressive development program must be undertaken if the mirrors are to achieve their intrinsic resolution and weight requirements by that time. Our tentative schedule for mirror development is summarized below:

| Milestone | Date |
|--|------|
| ----- | |
| Replicated Shell Mirror Mandrel and Related Development | |
| Complete 0.25 m polished mandrel | 1997 |
| Complete 0.5 m polished mandrels | 1997 |
| Complete 0.5 m mirror support structures | 1997 |
| High fidelity simulation of electroforming process, phase 1 | 1997 |
| Issue RFP to correct 0.5 m mandrel by ion polishing | 1998 |
| Investigate alumina (Al ₂ O ₃), molybdenum, tantalum mandrels | 1998 |
| Reduce 0.5 m mandrel diameter, repolish for CFRP replicas | 1998 |
| High fidelity simulation of electroforming process, phase 2 | 1998 |
| Machine modification to accommodate 1.3 m optics | 1998 |
| Correct 0.075 m mandrel by ion polishing | 1998 |
| Complete 1.3 m polished mandrels | 1998 |
| Complete Ion polish correction of 0.5 m mandrel | 1999 |
| Complete 1.3 m mirror support structures | 1999 |
| Reduce 1.3 m mandrel diameter, repolish for CFRP replicas | 1999 |
| ----- | |
| Replicated Shell Mirrors, Fabrication and Mechanical Tests | |
| Issue RFP for 0.5 m SiC carrier | 1997 |
| Complete 0.25 m Electroformed nickel mirror | 1997 |
| Complete 0.5 m thin electroformed Nickel mirror (without rings) | 1997 |
| Complete, mechanical test 0.5 m SiC, 2.0 mm walls | 1997 |
| Receive 0.5 m SiC carrier at MSFC | 1998 |
| Complete 0.5 m thin electroformed Nickel mirror with rings | 1998 |
| Issue RFP for 1.3 m SiC carrier | 1998 |
| Complete, mechanical test 0.5 m SiC, 1.5 mm walls | 1998 |
| Complete, mechanical test 0.5 m SiC, 1.0 mm walls | 1998 |
| Complete, mechanical test 0.5 m SiC, 0.5 mm walls | 1998 |
| Complete, mechanical test 0.5 m CFRP, 2.0 mm walls | 1998 |
| Complete, mechanical test 0.5 m CFRP, 1.5 mm walls | 1998 |
| Complete 0.5 m CFRP carrier using 0.5 m mandrel | 1998 |
| Complete, mechanical test 0.5 m CFRP, 1.0 mm walls | 1998 |
| Complete 0.5 m CFRP carrier mirror | 1998 |
| Complete 1.3 m thin electroformed nickel mirror | 1998 |

| | |
|--|------|
| Receive 1.3 m SiC carrier | 1998 |
| Complete 1.3 m SiC carrier mirror | 1999 |
| Complete, mechanical test 1.3 m SiC, 2.0 mm walls | 1999 |
| Vertical U.V. tests of 1.3 m electroformed nickel mirror | 1999 |
| Complete, mechanical test 1.3 m SiC, 1.5 mm walls | 1999 |
| Vertical U.V. tests of 1.3 m SiC mirror | 1999 |
| Complete, mechanical test 1.3 m SiC, 1.0 mm walls | 1999 |
| Complete, mechanical test 1.3 m CFRP, 3.0 mm walls | 1999 |
| Complete 1.3 m CFRP carrier using 1.3 m mandrel | 1999 |
| Complete, mechanical test 1.3 m CFRP, 2.0 mm walls | 1999 |
| Complete 0.5 m electroformed nickel mirror, ion polished mandrel | 1999 |
| Complete, mechanical test 1.3 m CFRP, 1.0 mm walls | 1999 |
| Complete 1.3 m CFRP carrier mirror | 1999 |
| Vertical U.V. tests of 1.3 m CFRP mirror | 1999 |

Replicated Shell Mirrors, X-ray Tests

| | |
|---|------|
| X-ray test, 0.075 m, thick electroformed nickel mirror | 1997 |
| X-ray test, 0.25 m electroformed nickel mirror | 1997 |
| X-ray test, 0.075 m thin electroformed nickel mirror with rings | 1997 |
| X-ray test, 0.5 m thick Nickel mirror (without rings) | 1997 |
| X-ray test, 0.5 m thin Nickel mirror with rings | 1998 |
| X-ray test, 0.5 m SiC carrier mirror | 1998 |
| X-ray test, 0.5 m CFRP carrier mirror | 1998 |
| Complete 0.5 m thin electroformed Nickel mirror (without rings) | 1997 |
| Complete 0.5 m thin electroformed Nickel mirror with rings | 1997 |
| X-ray test, 1.3 m electroformed nickel mirror | 1999 |
| X-ray test, 1.3 m SiC mirror | 1999 |
| X-ray test, 0.5 m nickel mirror, ion polished mandrel | 1999 |
| X-ray test, 1.3 m CFRP mirror | 2000 |

Segmented Mirrors, Mandrel Choice:

| | |
|--|------|
| Determine best performance using Pyrex mandrel set | 1997 |
| Procure and replicate polished metal mandrel set | 1997 |
| Procure and replicate polished glass mandrel set | 1997 |
| X-ray tests of reflectors from polished mandrels | 1997 |
| Computer feasibility study of ion figured foils | 1997 |
| Procure and replicate custom drawn Pyrex mandrel set | 1998 |
| Obtain/test second small (~40 cm) and large (~0.8 m) metal mandrel set | 1998 |
| Obtain/test second small and large glass mandrel set | 1998 |
| X-ray tests of second generation reflectors | 1998 |
| Demonstration of ion figured foils | 1998 |
| Assembly prototype for ion figured foils | 1998 |
| Obtain and replicate third prototype mandrel sets (metal and glass) | 1999 |
| X-ray tests of third generation reflectors | 1999 |

Select replication approach 1999

Segmented Mirrors, Fixturing:

| | |
|--|------|
| Fabricate and test most accurate alignment bars using EDM | 1997 |
| Fabricate and test diamond turned metal alignment bars | 1997 |
| Design, fab. and test alignment bars using micro lithography | 1998 |
| Fabricate and test refined metal alignment bars (2 sets) | 1998 |
| Fabricate micro lithographed alignment bars (2 sets) | 1998 |
| Select alignment bar fabrication technique | 1999 |

Large Diameter Foil Mirrors:

| | |
|---|------|
| Design 1 m mirror segment prototype | 1997 |
| Build and mechanically test prototype housing | 1998 |
| Build and test prototype mirror segment | 1999 |
| Build and test refined prototype segment | 2000 |

Final selection between segmented and replicated shell mirrors 2000

2.8 Existing Funding

2.8.1 Replicated Mirror Shells

The replicated mirror shell technology is supported as part of the optics program at MSFC. The current funding for X-ray optics development, including sub-contracts for mirror shells, is about \$600k per year. The MSFC optics group also supports facility and optical metrology standards development, studies for NGST and other programs, and the fabrication of flight hardware for the solar physics branch and rocket experiments. Most of this work is beneficial to the HTXS project. The OAB group is supported with European funds at a comparable level.

2.8.2 Segmented Foil Mirrors

The only explicit support for foil mirror development is a grant to the GSFC group through the high energy astrophysics SR&T program. While the overall goal of this program is the same as that of the HTXS program, namely the development of means for producing foil mirrors with spatial resolution approaching their theoretical limit, the amount of funding is very modest (\$50K per year). Consequently, this program is not expected to yield mirrors suitable for HTXS for many years. Additionally, the SR&T program is geared toward the development of small diameter mirrors. Thus there is no effort being expended towards the development of 1-meter class foil mirror. It is likely, however, that the segmented mirror development program will benefit from the X-ray optics program at MSFC, from which test mandrels might be made available.

3 X-Ray Calorimeters

3.1 Introduction

The low flux typical of most celestial X-ray sources requires a detector system that has the highest possible collecting area and efficiency. High resolution X-ray spectroscopy increases this need in proportion to the required spectral resolving power. The highest spectral resolution available has been with dispersive techniques that use gratings or crystal spectrometers. These offer extremely high energy resolution, particularly at low energies, but typically have low quantum efficiency and may not be suitable for the study of extended sources. Non-dispersive spectrometers, such as solid state Si detectors and CCDs have higher quantum efficiency but low energy resolution due to the relatively poor statistics associated with charge generation.

In 1983 a new approach to X-ray spectroscopy was developed that used the thermal detection of individual X-ray photons as a means of obtaining spectroscopic information (Moseley, Mather and McCammon, 1984). The X-ray microcalorimeter works by sensing the heat generated by X-ray photons when they are absorbed and thermalized in a very low heat capacity element. The temperature increase is a direct measure of the photon energy. In its simplest form, the temperature change resulting from absorbing an energy quantum E_x , is given by $\delta T \sim E_x/C$, where C is the heat capacity of the device. The temperature is restored to equilibrium exponentially with a time constant C/G, where G is the thermal conductance of the pixel to the cold bath.

A number of temperature-dependent effects can be exploited for use as a thermometer (see, e.g., Labov *et al.* 1996 and references therein). These include doped semiconductor resistance thermometers, devices that utilize superconducting transitions (either resistive or inductive), temperature-sensitive tunneling rate between a superconductor and normal metal, and the temperature dependence of paramagnetic susceptibility. All of these thermometer types have certain merits with regard to ultimate energy resolution over the 0.3 - 12 keV band pass, counting rate handling, ease of fabrication into large arrays, and operation in space. For the present purpose of demonstrating a clear path toward achieving a detector system with 2 eV resolution we must focus on approaches that have the highest margin of resolution performance against non-ideal effects, and which have shown the most amount of progress toward high resolution. In this discussion we will therefore concentrate on resistive microcalorimeters, which have achieved the highest resolution. Other approaches that evolve toward the requirements for HTXS must obviously be considered

The sensitivity of a resistive thermometer is characterized by the parameter

$$\alpha = |d(\log R)/d(\log T)|.$$

The fundamental noise processes that determine the energy resolution for an ideal microcalorimeter are Johnson noise originating in the resistive thermometer and phonon noise generated by the random exchange of energy (phonons) through the thermal link connecting the thermometer with the cold bath. The energy resolution (FWHM) theoretically achievable is given by $\Delta E = 2.35\xi\sqrt{k_B T^2 C}$, where ξ is a coefficient that scales as $1/\sqrt{\alpha}$ for $\alpha > 3$; for doped semiconductor thermometers α is in the range 3–6 and ξ is ~ 2 (Moseley *et al.* 1984). With the proper choice of materials the resolution of an X-ray microcalorimeter operating at a temperature of < 0.1 K can, in principle, be a few eV. This resolution is

independent of the X-ray energy to the extent that the temperature excursion of an event, $\delta T/T$, is small.

Recently, superconducting transition edge thermometers have been implemented in cryogenic detectors for particle and photon detection (Fergner *et al.* 1996; Irwin *et al.* 1996a). These have the advantage of very high values of dR/dT within the superconducting transition which result in very high values of α (up to ~ 1000), and thus higher energy resolution. For such a device, the value of ξ can be as low as ~ 0.1 (Irwin *et al.* 1996a). The much higher value of α improves other characteristics of the detector that will be discussed later.

In practice, microcalorimeters have two major components - the temperature sensing element and the X-ray absorber (see, e.g., Kelley *et al.* 1993). Normal metals provide excellent X-ray thermalization, but have a large electronic heat capacity. Instead, it has been found that some narrow gap semiconductors or semimetals (e.g., HgTe) work well as thermalizers, presumably because of the lack of a bandgap and the associated trapping sites that prevent charge recombination and the subsequent production of phonons.

In principle, the energy resolution of an ideal microcalorimeter is independent of its thermal conductance to the cold bath, and therefore the conductance can be chosen for the fastest pulse response. The physical processes by which photons are thermalized in solids should lead to very rapid thermal relaxation ($< 10\mu\text{sec}$), at least in non-superconductors. For microcalorimeters with semiconductor thermometers the thermal conductance is constrained by a number of effects that may prevent very high counting rates from being achieved. The heat capacities and thermal conductances of typical microcalorimeters have C/G time scales of the order of 1 msec, so counting rates of ~ 100 Hz per pixel should be possible before pulse pile-up effects degrade the energy resolution.

An important consequence of using resistive thermometers is the effect the changing resistance has on the pulse response. This is determined by how the detector is electrically biased. For a device with $dR/dT < 0$ that is current biased, the ohmic power dissipation drops as the pixel is heated and the temperature of the pixel is restored more rapidly than the thermal time constant, C/G . This is the negative electrothermal feedback case and speeds up the pulse recovery time by a factor that increases with α (Mather 1984). For a superconducting transition edge thermometer, with $dR/dT > 0$, the same effect can be obtained with voltage biasing and indeed the higher α can significantly increase the speed of the sensor.

3.2 Present Status of X-Ray Microcalorimeters

To date, most microcalorimeters have used either ion-implanted silicon or nuclear transmutation doped (NTD) germanium thermometers. The ion-implanted silicon thermometers have made it possible to use conventional microelectronic techniques to fabricate monolithic arrays of microcalorimeters. A silicon wafer is processed with a series of photolithographic masks and etching techniques to form a suspended structure that has an ion-planted thermometer and the required thermal conductance. Phosphorus and boron are typically used for the thermometer implant.

Most of the work done by the Goddard/Wisconsin group has been with arrays that have a simple linear geometry. The absorber area and thickness are chosen depending on the specific application. The pixels have absorbers with an area 0.5×2 mm and a thickness of

$\sim 0.7 \mu\text{m}$ to minimize the heat capacity while providing high efficiency up to 1 keV. The absorber is HgTe chemically vapor deposited onto $8 \mu\text{m}$ Si substrates, which are separately bonded to the Si pixel with epoxy. A 36 pixel array of microcalorimeters was recently flown on a suborbital payload to study the soft X-ray background (Cui *et al.* 1994 for a description of the payload; results from the flight are in preparation). The geometry of the array consists of two rows of 18 pixels. The energy resolution varied across the array from about 7 eV to about 20 eV at the C line. The prospects for improving the resolution for low energy applications are good. It should be possible to achieve ~ 2 eV with such a device by lowering the heat capacity of the thermometer system and improving the absorber attachment design (Stahle *et al.* 1996, 1997).

For the Astro-E/XRS instrument, to be launched in February 2000, two types of arrays are being developed in parallel. One is a smaller version of the bilinear array mentioned above and the other is a 6×6 pixel array (32 will read out in flight). The bilinear array uses absorbers with dimensions $0.3 \times 1.4 \text{ mm} \times 8 \mu\text{m}$ and the 6×6 array uses $0.63 \times 0.63 \text{ mm} \times 8 \mu\text{m}$. The fabrication of the 6×6 devices requires starting with relatively thin Si wafers ($75 \mu\text{m}$), which makes it difficult to achieve high production yields and the absorber attachment is more difficult than with the bi-linear arrays. Nonetheless an energy resolution of 10 eV has been achieved using a HgTe absorber with a volume comparable to the amount required for the XRS.

Alternatively, NTD germanium-based microcalorimeters can be constructed by integrating the thermometer with micromachined silicon structures. Since the impurity specific heat of doped germanium is approximately 50 times lower than that of doped silicon, the NTD germanium thermometer can be at least 50 times larger in volume relative to the implanted silicon thermometers. Consequently, the NTD thermometer can be used as a major structural element in the microcalorimeter, making it possible to build microcalorimeters where all of the thermalized X-ray energy flows from the X-ray absorber through the body of the sensor. This may improve the responsivity of the detector by fully redistributing phonons of all energies into a single temperature distribution. This fabrication technique lends itself to a simple array technology which involves bonding small chips of NTD to a metalized wiring pattern on a silicon nitride membrane. The X-ray absorbers would then be bump bonded, glued or electroplated onto a controlled area pedestal on top of the NTD sensor.

Using an NTD germanium-based microcalorimeter Silver *et al.* (1996) have achieved a resolution of 7.1 eV at 6 keV and an effective time constant of 0.5 msec with a Sn absorber of area 0.09 mm^2 . They have also operated devices with 0.2 msec time constants that have 10 eV resolution.

Most recently, Irwin *et al.* (1996b) have demonstrated a resolution of 7.8 eV at 6 keV using a Al/Ag transition edge sensor (TES) with a $0.25 \times 0.25 \text{ mm} \times 2$ micron silver absorber operating at 120 mK. The device had an effective time constant of 0.25 msec.

3.3 Limitations of Microcalorimeters with Semiconducting Thermometers

The thermal sensor uses the strong temperature dependence of the resistance, R , in semiconductors doped by either ion implantation or neutron transmutation. The crystal is doped to a density just below the metal-insulator transition (in the 50–100 mK range) and the

electron conduction mechanism is in the phonon-assisted hopping conduction regime. Over a wide temperature range the resistance follows the functional form $R = R_0 \exp(\sqrt{T_0/T})$ (Efros and Shklovskii 1975) and the sensitivity parameter, α , is given by $\frac{1}{2}\sqrt{T_0/T}$. The value of T_0 is extremely sensitive to the net density of the implanted ions. For low densities T_0 is high and the resistance and temperature sensitivity are also high. However, as the value of T_0 increases, the allowable power density in the thermometer drops (McCammon *et al.* 1993). Since there exists an optimum bias power for maximum energy resolution (such that the sensor is about 12% warmer than the thermal sink; Moseley *et al.*, 1984), this translates into a lower limit on the volume, and therefore heat capacity, of a doped semiconductor thermometer. This effect is widely thought of as a decoupling between the electrons in the thermometer system and the lattice. The problem can be offset by lowering the thermal conductance of the support beams, which would lower the optimum bias power, but then the thermal response time would increase and the sensor would become more sensitive to absorbed power that is radiated (e.g., IR) or conducted into the thermometer through wiring. For higher net densities, the value of T_0 and resistance are decreased and the device becomes insensitive simply because of the smaller value of dR/dT .

Ion-implanted thermometers can also exhibit current noise. As the bias voltage is applied to the sensor, voltage noise in excess of the thermometer Johnson noise appears that is proportional to the current flowing through the thermistor. This noise component has a 1/f power spectrum and a magnitude that scales inversely with the square-root of the volume of the ion-implanted area and with the thermometer sensitivity (McCammon *et al.* 1993).

The overall optimum value of T_0 , and ultimately the energy resolution, are determined by an optimum size and net density for ion-implanted thermometers and thermal conductance that minimizes the effects of thermistor heat capacity, thermistor decoupling, and current noise. A quantitative tradeoff has yet to be fully completed, and it is likely that significant improvements can be achieved with microcalorimeters using doped semiconductor thermometers. At the present time, a value for $T_0 \sim 6$ K and a thermal conductance of $\sim 4 \times 10^{-11}$ W/K at 0.1 K appears to be about optimal with respect to these effects in ion implanted Si microcalorimeters.

3.4 Absorbers for Semiconductor Thermometer Calorimeters

The choice of an absorber for a microcalorimeter with a semiconductor thermometer is determined by a number of effects. In general, the optimum choice for the absorber is a material that has the highest X-ray opacity per unit heat capacity. This would allow the largest volume of material to be used for a specified quantum efficiency and energy resolution. This larger volume can be used to increase the quantum efficiency at higher energies by making the absorber thicker or to increase the area of the pixel to obtain a larger field-of-view. However, as the heat capacity of the absorber is reduced, the fractional temperature change of the microcalorimeter, $\delta T/T$, increases as approximately $1/C$ and the pulse amplitude will become non-linear with increasing energy. This introduces a non-linearity in the pulse response that degrades the energy resolution with increasing energy. There is thus an optimum heat capacity depending on the energy band of interest and other detector parameters, such as the heat capacity of the thermometer system.

Superconductors have long been recognized as potential candidates for X-ray absorbers. Well below the superconducting transition the electronic specific heat freezes out leaving

only the lattice Debye heat capacity, which scales as $(T/\Theta_D)^3$, where Θ_D is the Debye temperature. Superconducting tin has worked well as an X-ray absorber in bulk form and has a heat capacity that is 2.6 times lower than HgTe. High Z superconductors such as Os and Re should have much lower heat capacity and could ultimately be used for large volume absorber applications, but there are reasons to expect that superconductors with high Θ_D may not work well as X-ray thermalizers for microcalorimeters (e.g., Zehnder 1995). Indeed tests with Re have generally produced worse results than HgTe and Sn absorbers. A long, secondary time constant on the pulse response is generally found and poor resolution. This behavior suggests an additional, weakly coupled heat capacity (it is difficult to obtain high-purity samples of refractory metals such as Re), or long recombination times that broken Cooper pairs (\sim free electrons or quasiparticles) can have at temperatures below 0.1 K. There are techniques that can be applied to assist quasiparticle recombination if this is the major problem. Tests of Ta films with a layer of Au to promote quasiparticle recombination have shown promise but have not been repeatable.

One of the most important aspects in determining the performance of an X-ray microcalorimeter is how the absorber is attached to the thermometer. Epoxy is most often used and has a large specific heat. Using microscopic quantities of epoxy can be problematic for controlling the mechanical and thermal properties of the bond. For example if the thermal conductance is too high, a position dependence to the pulse response may arise due to the finite thermal conductance across the absorber. Other bonding techniques, such as indium bump bonding, are being investigated.

3.5 New Technologies for Semiconductor Thermometers

A promising new silicon thermometer technology, epitaxially grown doped silicon thermistors, has emerged from the observation that the low temperature growth conditions used during the manufacture of epitaxial silicon may produce a superior silicon thermistor. The process has the added advantage of high uniformity and reproducibility over large areas and may develop into an efficient, inexpensive, silicon microcalorimeter array technology. The epitaxially grown layers offer a high degree of dopant activation, which may yield a lower heat capacity thermistor. At the very least, this offers a range of doping and geometric parameters inaccessible to ion implantation and neutron transmutation methods.

Starting with a substrate of high purity silicon, a layer of epitaxial silicon is grown by means of chemical vapor deposition. The doping of the epitaxial layer takes place in the vapor phase of the processing. Measurements have demonstrated that the gradients of resistance vs. temperature are of the same order as the best currently found in NTD germanium. However, this technique offers a greater range of dopant concentration without damage to the crystals (from ion implantation) and a greater range of compensation doping than is possible in NTD germanium. This opens the possibility for tuning the responsivity, α , for the desired temperature range and perhaps lowering current noise.

The doped epitaxial layer is grown on a silicon substrate and is therefore in intimate contact with it. Common solid-state etching procedures can be used to design the size and shape of the epitaxial thermistor. These epitaxial layers have been grown on three inch diameter silicon wafers making it possible to extract hundreds of thermal sensors. Epitaxially-doped Ge on a pure Si substrate is also being pursued. Ge may be preferred over Si for the detector matrix because the dopant heat capacity per unit volume is significantly lower in

the former, allowing larger thermistors. Epitaxial Ge offers the same advantages as epitaxial Si as a sensor material: increased flexibility in optimizing performance and in producing integrated detector arrays. A Si-Ge buffer layer with graded composition is grown on a silicon substrate, and a doped epitaxial Ge detector layer is then grown on the buffer layer.

3.6 Superconducting Transition Edge Thermometers

Many of the limitations that have been identified with semiconductor thermometers can potentially be overcome with a thermometer that can achieve much higher α . The use of a superconducting transition edge thermometer operating in extreme negative electrothermal feedback mode has been explored in detail and substantial experimental work is now under way by Irwin *et al.* (1996a,b). With values of α as high as 1000 (already achieved) it should be possible to improve the energy resolution by an order of magnitude over existing microcalorimeters. A large value of α allows a greater margin on heat capacity. Indeed the small temperature range of the transition requires a minimum heat capacity large enough to keep the temperature excursion within the transition. This minimum is larger than the heat capacity of the XRS calorimeters yet the device can still deliver higher resolution because of the much higher value of α . A normal metal can now be considered as a practical absorber.

Beside the improved energy resolution made possible with a transition edge sensor is the associated improvement in detector speed. The higher level of electrothermal feedback decreases the pulse response time by a large factor (> 100) compared to C/G, allowing significantly higher counting rates to be handled before pile-up effects degrade the energy resolution. The stable feedback may also allow some relaxation of the temperature stability of the heat sink.

The low impedance of the sensor means that a SQUID (Superconducting QUantum Interference Device) amplifier can be used. This is the lowest noise current amplifier available and could also significantly reduce the amplifier heat load into long-duration cryogenic systems compared with the JFETs required by semiconductor thermometers. The low impedance (typically less than an ohm) also means that the sensitivity to capacitively coupled microphonics would be reduced.

It may be possible to fabricate large monolithic arrays of TES microcalorimeters by using electron-phonon decoupling or boundary resistance as the thermal link to the heat sink rather than delicate etched Si structures currently in use. This would depend on the ultimate temperature of operation. The larger heat capacity budget means that normal metals can be used for the absorber, which are easily deposited and could contribute to simplified array fabrication.

3.7 Larger Arrays of Microcalorimeters

The long focal lengths likely required for the next generation of X-ray observatories means that large focal plane arrays are necessary in order to subtend a reasonable field-of-view. An X-ray mirror system with an 8 meter focal length will have a plate scale of $26''/\text{mm}$. This means that a $10' \times 10'$ FOV would require an array size of 23 mm on a side. For comparison, the array being developed for the Astro-E/XRS measures less than 4 mm on a side. To achieve larger fields-of-view with pixel sizes that at least partially over-sample

the point spread function of the mirror will require arrays with 5" pixels (0.2 mm on a side). For a 2.5' FOV, a 30 x 30 pixel array is required and a 10' FOV requires a 120 x 120 pixel array. To achieve such array sizes necessitates the development of absorber schemes that are integral to the device fabrication and multiplexed amplifier schemes. Consideration will also have to be given to minimizing cryogen heat loads through proper isolation and anchoring of co-located electronics (e.g., JFETs and SQUIDs) and the down-stream digital electronics for dealing with so many channels. Emphasis should probably be placed on array fabrication that is based on building up large arrays from small sub-arrays that can be pretested and screened.

3.8 The Path Toward Higher Spectral Resolution

Higher spectral resolution should be achievable by pursuing both existing semiconductor thermometer microcalorimeters and especially the transition edge sensors. The theoretical resolution of microcalorimeters with semiconductor thermometers is a few eV (at least at lower energies) and has not yet been realized. Improvements in these devices will require careful optimization of the thermometer parameters and improving the absorbers and absorber attachment. These problems may be obviated by the rapid progress on transition edge sensors and higher speed SQUIDs. The ultimate resolution of these devices will probably depend on the extent to which non-ideal effects can be controlled, but at the present time it appears that significant improvements in resolution can be achieved and that this approach should be vigorously pursued. An energy resolution of better than 8 eV has already been reported and the prospects are good for substantial near-term improvement.

3.9 References

- Cui, W., *et al.*, 1994, SPIE, 2280, 362.
- Efros, A.L. and Shklovskii, B.I., 1975, J Phys, C8, L49.
- Ferger, P., *et al.*, 1996, NIM Phys Res A, 370, 157.
- Irwin, K.D., *et al.*, 1996a, NIM Phys Res A, 370, 177.
- Irwin, K.D., *et al.*, 1996b, Workshop on High Throughput X-ray Spectroscopy, Boston, Sept. 30-Oct. 1, 1996.
- Kelley, R.L., *et al.*, 1993, J Low Temp Phys, 93, 225.
- Lebov, S.E., *et al.*, 1996, NIM Phys Res A, 370, 65.
- Mather, J.C., 1984, Applied Optics, 23, 584.
- McCammon, D., *et al.*, 1993, NIM Phys Res A, 326, 157.
- Moseley, S.H., Mather, J.C., and McCammon, D., 1984, J Appl Phys, 56, 1257.
- Silver, E., *et al.*, 1996, X-Ray Spectrometry, 25, 115.
- Stahle, C.K., *et al.*, 1997, Proc. STAIF-97, Jan. 26-30, 1997, Albuquerque, NM.

Stahle, C.K., *et al.*, 1996, NIM Phys Res A, 370, 173.

Zehnder, A., 1995, Phys Rev B, 52, 12858.

3.10 Metrics

1. Use existing microcalorimeter technology with a low heat capacity absorber to demonstrate that 2 eV resolution is indeed feasible using microcalorimeter technology.
2. Optimize the sensitivity parameter, α , for ion-implanted, NTD and doped epitaxial silicon/germanium thermometer microcalorimeters. Specifically, determine the optimum thermometer area, thickness, aspect ratio, value of α and thermal conductance for maximum signal-to-noise.
3. Measure the X-ray thermalization of superconductors with low Debye heat capacity and high opacity (e.g., high quality samples of Os and Re).
4. Establish the best absorber for microcalorimeters with semiconductor (i.e., ion-implanted Si or NTD Ge) thermometers.
5. Quantify the tradeoff between highest energy resolution and counting rate handling capacity and incorporate this into the design of subsequent microcalorimeter arrays based on evaluation of likely X-ray optics (collecting area and point spread function).
6. Fabricate small microcalorimeter arrays with semiconductor thermometers and optimal absorber material to establish the best possible energy resolution.
7. Fabricate larger format microcalorimeter array (e.g., 10 x 10 or greater) based on this technology to establish the readiness of large array technology.
8. Develop integrated SQUID arrays or multiplex schemes to allow for reading out large numbers of TES pixels.
9. Fabricate small number TES arrays to establish energy resolution performance.
10. Fabricate large format (e.g., 30 x 30) TES arrays to establish readiness of array technology.

3.11 Mission Criticality

The development of a microcalorimeter array with an energy resolution of ~ 2 eV is critical to the success of HTXS. In addition, the high quantum efficiency simultaneously over the full 0.3 - 12 energy band pass coupled with pile-up free throughput of 100 Hz per pixel is essential for the success of the mission.

3.12 Milestones for Calorimeter Development

| Milestone | Year |
|--|-------|
| Phase 1: | |
| Fabricate operational microcalorimeter array designed to achieve 2 eV resolution below 1 keV | 12/97 |
| Fabricate operational TES devices with 2 eV resolution above 1 keV | 09/98 |
| Demonstrate SQUID amplifier readout scheme appropriate for instrumenting a 30 x 30 TES array | 12/98 |
| Fabricate test devices to map out parameter space for the noise and sensitivity performance of ion-planted silicon and NTD germanium thermistors | 12/97 |
| Fabricate epitaxial silicon thermistors | 03/98 |
| Incorporate superconducting X-ray absorbers into calorimeters using silicon or germanium thermistors and evaluate performance | 06/98 |
| Fabricate operational semiconductor microcalorimeter with 2 eV resolution above 1 keV | 09/98 |
| Demonstrate FET amplifier assembly appropriate for instrumenting a 30 x 30 semiconductor calorimeter array | 12/98 |
| Select primary technology | 06/99 |
| Phase 2: | |
| Develop bread board model of 30 x 30 array with primary technology | 12/99 |
| Final selection of technology for HTXS | 12/00 |

4 The Reflection Grating Array

4.1 Introduction

The baseline reflection grating spectrometer design for HTXS involves an array of thin reflection gratings mounted at grazing incidence to the beam immediately behind the Spectroscopy X-Ray Telescope optics. The grating array covers only the outer half of the telescope shells and the gratings are spaced so as to "pick off" only $\sim 50\%$ of the light passing through. The remaining 50% of the light from the outer shells, and all of the light from the inner shells, passes undeflected through the grating array to the quantum micro-calorimeter at the telescope focus. The light picked off by the gratings is dispersed to a strip of CCD detectors offset in the dispersion direction at the telescope focal plane. The gratings are all mounted at the same incident graze angle with respect to the ray passing through grating center, and they are positioned on a Rowland torus which also contains the telescope focus and the CCD detectors. This configuration eliminates the comatic aberrations which would otherwise result from the array geometry. There are additional aberrations caused by the convergence of the beam intercepted by each individual grating. These are removed by slightly varying the groove spacing over the length of the grating.

The spectral resolution of the spectrometer is determined by a number of factors, including (in descending order of importance): (1) the angular resolution of the telescope, (2) the flatness of individual gratings, (3) the relative alignment of individual gratings within the array, (4) the accuracy of the groove spacing, and (5) the spatial resolution of the detector. To achieve the desired resolution for HTXS, all terms except the first should be kept as small as possible. This requires \sim arc-second flatness for the as aligned gratings, and \sim arc-second positioning and stability within the overall array. The latter leads to positional tolerances at the level of ~ 1 micron or so.

The other science performance aspects of the spectrometer are determined by the quality of the rulings on the individual gratings. In particular, the diffraction efficiency as a function of wavelength (directly proportional to the effective area) is determined by the mean groove profile. Maximal efficiency for a desired central wavelength is obtained for a "blazed" profile, where the groove is triangular in shape, i.e. the groove "facet" is tilted at a particular angle, the "blaze angle", relative to the grating plane. For the design parameters of HTXS, this blaze angle is ~ 1 degree, and the mean line spacing is ~ 2 microns, so the groove height is only ~ 400 Angstroms. Nonuniformities from groove to groove can lead to small angle scatter, which can lead either to a degradation in resolution or a loss of efficiency, depending on spatial scale. Finally, microroughness within a groove leads to large angle scatter, which both decreases the diffraction efficiency and increases background.

4.2 Current Status

The baseline design described above follows closely the design adopted for the Reflection Grating Spectrometer (RGS) under development for XMM by Columbia University, and, to a significant degree, the requisite technology has been demonstrated in connection with that program. The RGS gratings are produced by epoxy replication onto thin SiC substrates, which are machined to the required flatness from hot, isotatically pressed SiC blocks. The substrate geometry involves a thin face sheet with several "ribs" on the rear side, oriented

along the direction of the incoming light for minimal obscuration, that provide added stiffness in the critical direction. The gratings are mounted against four coplanar "bosses", which are precision-machined into alignment rails that are, in turn mounted and aligned on a monolithic integrating structure. The tolerances on the boss positions are +/- 1.25 microns. The integrating structure is fabricated from a billet of I-250 grade beryllium, which has been lightweighted using electrical discharge machining to minimize residual stress. The total grating array mass for the XMM-RGS is 60 kg, roughly 20 kg of which is taken up by the gratings themselves.

For HTXS the principal technical challenge associated with this baseline design will involve scaling to considerably larger area without incurring the expected linear extrapolation in mass and cost. In addition, a rather different approach to the fabrication of the integrating structure may be appropriate, given that the array is planned to cover only an outer annulus of the telescope mirror shells. Mass and cost reduction, with no loss in alignment precision, is the key technical driver. In this context, other materials choices should be investigated, as detailed below.

A second technical challenge will involve improving the scientific performance of the gratings, particularly in terms of efficiency and scattering. For XMM, master gratings were fabricated by two different processes: (1) direct mechanical ruling into a gold coating; and (2) holography followed by ion etching onto a glass substrate. The mechanically ruled master (which is being used for the flight gratings) exhibited good fidelity to the desired groove shape, but only ~ 70% of theoretical diffraction efficiency, and significant scatter, indicative of roughness at the 10 Angstrom level or higher. The holographic grating exhibited near theoretical diffraction efficiency in first order, and low scatter, but some errors in the line spacing, which could lead to ghosts and or resolution degradation. In addition, a change in blaze angle was encountered during the replication process, indicative of grating "fatigue" due to excessive replication. This could be a serious issue for HTXS given the large number of gratings which will be required. Clearly, further technology development in the area of master grating fabrication and/or replication is warranted.

4.3 Technology Requirements

4.3.1 Mass Reduction

For significant mass reduction over the XMM design, further lightweighting must be achieved in both the integrating structure which holds the gratings, and in the gratings themselves. We discuss these two aspects separately below.

1. *Lightweighting the integrating structure.* For XMM, the reflection grating array is a separate deliverable unit, designed specifically for minimal interfaces with the design of the telescope module and the rest of the spacecraft. As such, it contains its own integrating structure which is kinematically mounted to a support ring attached to the telescope. For HTXS, a more "holistic" design can be envisaged, wherein the telescope and grating arrays form a single integral optics package with a single integrating structure. This requires design iteration and finite element modeling for the two components. A full spectrum of possible materials choices should be considered, including beryllium, advanced ceramics, metal matrix composites, and carbon-fiber

reinforced plastics.

2. *Lightweighting the gratings.* The alignment approach adopted for XMM, wherein the individual gratings are mounted against four coplanar precision bosses, suggests that the gratings need not necessarily be rigid, stiff structures. As such, replication onto very light, flexible carriers, like mylar films, or glass microsheets might be possible. This has not yet been attempted for X-ray diffraction gratings, although thin mylar reflection gratings and other microstructures have been fabricated for optical applications. Issues that must be investigated are the fidelity of the replication process on flexible films, and the flatness and removal of "ripples" in the as-mounted configuration. Use of such alternative substrates could also lead to substantial cost reduction for the production of the large number of gratings required.

4.3.2 Improved Scientific Performance

As discussed above, the scientific performance of the gratings is primarily a function of the groove properties, which are in turn determined by the master fabrication process and the method of replication. Improvements over XMM might be expected from alternative methodologies. One exciting possibility involves the direct fabrication of the gratings via advanced scanning beam techniques, as developed, for example, at the Space Microstructures Laboratory at MIT. Atomically smooth grating facets with near perfect blazed groove profiles and no roughness may be feasible with this approach. In addition, gratings can be produced directly onto thin silicon wafers, so that replication may not be required to produce the large number of gratings necessary to fill the array.

4.4 Metrics

The metrics for the technology development in the reflection grating array follow directly from the requirements discussed above. In the area of weight reduction, we are looking for a factor 3-4 reduction of mass per unit area over that achieved by XMM, with no loss in alignment precision or stability. In the area of scientific performance, we are looking for $\geq 95\%$ of theoretical diffraction efficiency with scatter indicative of roughness at the 3 Angstrom level or less.

4.5 Mission Criticality

The reflection grating spectrometer is essential for the scientific objectives of the HTXS mission, so as to ensure that the requisite spectral resolution and effective area can be achieved in the line-rich spectral range below 1 keV. Significant weight reduction over the XMM design is required to meet the design weight for the grating component of the payload.

4.6 Milestones for Grating Development

| Milestone | Date |
|--|------|
| ----- | |
| Mass Reduction Program: | |
| Design of integral integrating structure for telescope and grating array | 1997 |
| Development of replication onto lightweight, flexible substrates | 1999 |
| ----- | |
| Scientific Performance Program: | |
| First fabrication of prototype gratings using scanning beam techniques | 1997 |
| Investigation of production fabrication of gratings | 1998 |
| ----- | |

5 CCDs

5.1 Introduction

CCDs are relatively mature technology, having been used on at least a dozen current and developing missions. Science grade CCDs, especially those of use to X-ray astronomy, are still not off-the-shelf items. In addition to the existing needs for excellent background rejection, ultra-low readnoise, and good low energy quantum efficiency, the HTXS mission will place an extreme premium on low power, and low weight with chip formats that are optimized for grating spectroscopy readout.

The low power requirement can primarily be met by decreasing the overall "pixel rate", through reducing the number of pixels in the cross-dispersion direction as well as decreasing the frame rate. Pixel dimensions for optimal sampling are also quite large for HTXS; furthermore, the pixels should be rectangular in shape. Since the chips do not have to have as high intrinsic spectral resolution as imaging spectrometers require (because the intrinsic resolution is only used for order separation) the larger pixel's effect on combining single events and split events is tolerable.

Low-energy quantum efficiency has been problematic for CCD developers. Two competing techniques are currently in use to achieve enhanced low-energy response. The AXAF ACIS and XMM RGS programs are using back-side illuminated (BI) devices. In this approach the CCDs are fabricated much the same as a normal front-side CCD, but a final thinning stage removes the substrate material from the back of the CCD, until only depletion region material remains. Then if the CCD is illuminated from this backside the only absorbing material an incident X-ray sees is a tiny (tens of Angstroms thick) native oxide layer, which forms on the silicon. Although this approach offers the theoretical best efficiency, the demonstrated device yield of the backside fabrication process is very low. The RGS BI chips exhibit a 2000 Å layer of incomplete collection efficiency, and the ACIS BI chips have an unexplained poor energy resolution below 1 keV.

A second approach to improving low energy quantum efficiency has been pursued for the XMM EPIC experiment. Rather than trying to thin the backside of the chip, one of the MOS gate structures is made exceedingly thin. As this gate can cover up to 2/3 of the CCD area, it offers a substantial improvement at low energy. By using multiple samplings of the same charge packet, it is possible to reduce readnoise to less than one electron rms, allowing single photon detections at Al L and Si L (recently reported by the Penn State group). The current device is not suitable for flight because the multiple readouts must utilize the same output sampling circuitry, slowing the effective readout rate to impractical levels.

A third approach to improving low energy quantum efficiency has recently been proposed by the MIT group. Based on a novel, ultrathin resistive-gate CCD (RGCCD) geometry, this approach naturally produces a rectangular pixel geometry, and operates with device and clocking power levels 10-20 times lower than conventional MOS devices. Yield levels for the RGCCD process are very promising, based on the two-fold reduction in the number of processing steps and the immunity of the RGCCD to interlevel shorts. Readout noise levels of less than 1 electron RMS should be readily achieved. The RGCCD design is intrinsically radiation hard, since the only significant trapping losses will occur under doped gate regions, which occupy less than 5% of the device area. Thus, RGCCDs should be more than an order of magnitude harder to displacement damage than are conventional MOS CCDs.

We propose to follow a two-pronged approach to develop the new CCD designs that HTXS needs. One approach will pursue thinned-gate CCDs with serial charge sampling output gates suitable to high readout rates. Another approach will develop the RGCCD. Both programs will perform these developments on CCD formats which will be aimed at the needs of the HTXS grating readout, i.e. low power and long formats in the dispersion direction.

The ACIS and XMM RGS CCD programs have produced only a handful of flyable BI devices, albeit with excellent low energy quantum efficiency, roughly a factor of two times better than conventional front-side CCDs. Both the XMM EPIC (demonstrated) and RGCCD (estimated) approaches provide low energy quantum efficiency a factor of 1.5–1.7 times better than conventional front-side CCDs. It is our view that the larger number of low energy-sensitive CCDs required for HTXS (5–6 times more than AXAF) mandate development of more robust processing technologies than used in producing thinned, back illuminated CCDs. All technologies for producing thinned, BI CCDs of which we are aware incorporate uncomfortably large amounts of incompletely understood "black art", which tends to rely on the expertise of 1 or 2 key people. Achieving a scientific understanding of the BI CCD recipe, and providing for the transfer of the knowledge to production of flight devices 5–7 years in the future (necessarily using a later generation of semiconductor fabrication facilities) would require an extraordinary commitment of resources, and entail high programmatic risk. Hence, we do not recommend the BI CCD approach for HTXS.

HTXS will benefit greatly from the use of thin optical blocking filters (OBFs), since only diffracted light will strike the CCDs. We also plan to experiment with techniques for direct deposition of filter material on the CCDs, which can reduce the X-ray attenuation by OBFs even more.

5.2 Metrics

The specific goals of CCD development needed for HTXS are clear. The program must deliver chips which will equal the ACIS/EPIC CCDs in depletion depth (60 microns ; for background rejection and high energy quantum efficiency), deliver at least the equivalent of four electrons readnoise energy resolution (120 eV at 6 keV; 55 eV at 1 keV); and provide low energy quantum efficiency comparable to the ACIS back-side illuminated CCDs (50% at 0.5 keV).

The HTXS CCD cameras and signal chains must provide excellent performance, yet require much lower mass and power than those of previous missions. A promising systems approach is to establish metrics on the camera designs (which will critically depend on the chip characteristics). Optimization will include trading off numbers of readout signal chains, the degree of multiplexing in processors, and complexity in synchronizing readouts.

Thus, the weight and power metric for the HTXS CCD array will require a camera design based on a total power of less than 20 W, and a mass limit of 50 kg, for a CCD array 245 mm in length. (The power is ten times lower than AXAF, the mass more than two times lower and the linear extent is 5/3 the AXAF maximum extent.)

5.3 Mission Criticality

The CCD/grating combination is central to the low energy 0.25–1.0 keV spectral performance of the HTXS mission. If the optimum calorimeter is developed the cross-over occurs at 1 keV. Enormous numbers of X-ray lines are found in this spectral region, including the O line complex (arguably the dominant X-ray line in the Universe) and the Fe L line complexes, critical for understanding of the K line counterparts. If the calorimeter is unable to meet the 6 eV goal, a fall back will be to reoptimize the grating to operate up to higher energies. For example with a more conservative 6 eV prediction the cross-over point of the energy resolution between the CCDs and calorimeter occurs at 2 keV.

The CCDs also provide a longevity to the mission after the cryogen is exhausted on the calorimeter because the CCDs have no expendables. Experience from the ROSAT and Einstein missions has shown that significant useful scientific results have been achieved by operating the mission with the long-lived instruments after the expendables have been consumed. The ROSAT HRI has continued operations for several years after the PSPC ran out of gas; the Einstein mission similarly functioned after the SSS ran out of cryogen.

Unless the required improvements in CCDs are provided, a mission profile which accommodates the full package of CCD/XRS/HXT may not be possible, which compromises the scientific balance of the mission.

5.4 Milestones for CCD Development

Timeline and milestones for Resistive-Gate Charge-Coupled Devices (RG) CCDs.

- FY 1997 Begin design work on a mask set comprising several design options for the device and a variety of process test structures; Begin process experiments to produce resistive polysilicon layers of the desired sheet resistivity; Measure existing test devices that incorporate perimeter guard rings that allow biasing of the substrate.
- FY 1998 Begin processing a 22-wafer lot of the new design; Complete first lot and conduct initial wafer probing (shorts/opens tests at room temperature); Second set of wafer probing tests at temperatures down to about -60C to measure charge-transfer inefficiency (CTI) and dark current; Package sample devices in standard 72-pin kovar package; Design custom analog chip incorporating a correlated double sampler and a level discriminator.
- FY 1999 Fabricate a second lot of RGCCDs, incorporating the best choice of design parameters established from testing the first lot of devices; Package samples and test for radiation hardness using 40 MeV protons; Fabricate and test custom analog chip.
- FY2000 If selected as the baseline approach then fabricate a third lot of RGCCDs; Fabricate sample RGCCD focal plane; Assemble and test breadboard electronics; Evaluate performance (mass, power, noise) with sample RGCCD focal plane.

Timeline and milestones for thinned-gate, multiple Floating Gate Amplifier (FGA) CCDs.

- FY1997 Complete CCD design and camera analog electronics design; Design, build and test improved low noise FGA outputs; Demonstrate serial FGA output on small test CCDs; Evaluate thin-gate structures with large pixels on small test CCDs.
- FY1998 Fabricate first lot of flight prototype CCDs.
- FY1999 Complete scientific evaluation of first lot; Fabricate second lot of flight prototype CCDs; Complete scientific evaluation of second lot of CCDs.
- FY2000 If selected as the baseline approach then fabricate sample FGA CCD focal plane; Assemble and test breadboard electronics; Evaluate performance (mass, power, noise) with sample FGA CCD focal plane.

The technology development approach will be to pursue both technologies along parallel paths, and make a final selection in December 1999. This selection will be based on meeting the required performance and may be moved forward if the technology is not meeting expectations. At the present time, the RG CCDs appear to be the most promising and this will be used as the baseline to be pursued. We will also maintain an FGA CCD development program as a fall back option.

6 The Cryogenics Subsystems

6.0.1 Technology Requirement

The HTXS instrumentation includes X-ray calorimeters which must operate at a temperature of approximately 65 mK, attained through active cooling. Six individual but identical satellites are proposed for the mission and will be launched sequentially every three to four months into an L2 orbit. To achieve a reasonable total science mission, a 5 year lifetime on expendables (including stored cryogenics) is required for each satellite. A Delta 7925 H has a lift capability of 1600 kg to L2, with a 9.5 ft fairing. The dimensions and capability of the Delta 7925 H impose restrictions on the HTXS mission by requiring minimization of mass and volume of all components. To meet these requirements, we propose the use of a mechanical cooler to decrease the mass and size of the stored cryogen system, while simultaneously extending the lifetime. It should be noted a mechanical cooler with virtually identical requirements is required in the Origins program.

6.1 The Possible Options

The cryogenic subsystem of HTXS must provide the sub-Kelvin operating temperature required by the calorimeters, within a fairly severe envelope of weight, power, size and cost constraints. While a system like that being created for the Astro-E X-ray Spectrometer (XRS) could be developed to meet the HTXS requirements, it would consume a large fraction of the available resources, and would be the system which limited the duration of the mission. In this section we outline our planned investigations for development of the technologies that would permit the construction of simpler, longer-lived cryogenic systems.

There are three main subsystems involved in the existing XRS cryogenic design; a solid neon dewar to provide cooling from ambient down to 17 K, a superfluid helium cryostat to provide cooling from 17 K to 1.4 K, and an adiabatic demagnetization refrigerator (ADR) to provide cooling from 1.4 K down to 0.065 K. Such a dual-cryogen system, similar to the XRS design, was studied for use on HTXS as currently available technology. The L2 orbit provides a major benefit to the lifetime, because it moves the cryostat far from the warming influence of the Earth. Outer shell temperatures of $\sim 170\text{K}$ can be achieved, compared to 230–240K in low earth orbit. The simplest design for HTXS consists of a 330 l dewar of superfluid helium with three vapor cooled shields with an ADR used to achieve the 65 mK for the detectors. This design, similar to one being used for the SIRTf mission, utilizes immediately available technology and would be capable of achieving the required 5 year lifetime, but at cost of weight and overall size which could limit mission capability.

We are considering two options for improved cryogenic cooling systems for HTXS:

1. Option 1: A mechanical cooler is used to intercept much of the external heat load onto the helium cryostat. Such a system could be smaller and lighter, at the cost of increased power, but its lifetime would still be limited by consumption of the helium.
2. Option 2: The helium cryostat in option 1 is replaced by a more advanced mechanical cooler, delivering lower temperatures. This second cooler would be used as the first cooling stage for an advanced sub-Kelvin system which would probably have to reject heat at a higher temperature.

A system using the first option could be available by the end of 1999 while a system using the second might not be available until the end of 2002 (although could be accelerated if sufficient resources were allocated). The first option is sufficient to meet the weight and lifetime requirements of HTXS.

There are several forms of mechanical coolers which could be used. All of them function by compressing a working fluid, allowing the compressed fluid to equilibrate with a heat sink, moving the fluid to the cold end, allowing the fluid to expand, and then having the fluid absorb heat. At least two coolers with high potential of meeting the HTXS requirements are under development, a miniature turbo-Brayton cycle cooler and a sorption cooler.

The turbo-Brayton machine is a recuperative type cooler, using counterflow heat exchangers to exchange the heat between the working fluid leaving the cold end and the working fluid approaching the cold end. Recuperative cycle coolers do not require reciprocating parts, but instead utilize turbines that do not produce the appreciable levels of vibration produced by regenerative type machines such as the Stirling cycle coolers. A 65 K turbo-Brayton cycle cooler is currently undergoing life test and a critical technology demonstration is planned for components of a 6 to 8 K version in 1997. If this technology demonstration is successful, the 6 to 8 K cooler could be made ready for flight production by the year 2000.

Sorption cooling works by sequentially heating and cooling a specialized metal alloy powder that absorbs the refrigerant. The powder is heated to pressurize the refrigerant, then cooled to reduce the pressure, circulating the refrigerant through the system. The refrigerant is expanded, using Joule expansion, at the cold, producing the final cooling temperature. A technology demonstration of a 10 K, continuously operating sorption cooler is planned by JPL for FY97.

In addition, we will continue to investigate alternate coolers, such as Stirling coolers. In the Stirling cycle coolers being developed, the compression and expansion are performed with pistons, or diaphragms. Two-stage Stirling coolers can achieve temperatures of 35 K and there is the possibility of reaching 20 K if the heat rejection temperature is reduced to approximately 200K, which would be feasible in the orbits being considered for HTXS.

6.2 Success Criteria

The first success criteria for both systems is to provide a stable operating temperature of nominally 0.065 K for the detector array. The second success criteria for both approaches is a system with a highly reliable lifetime of at least 5 years. The third requirement is to deliver a system within the weight budget of the mission.

The first system accomplishes these goals by limiting the heat input to the stored liquid helium system and dramatically reducing the volume of cryogen. The first system will have a total mass of < 130 kg (8 kg for the turbo-Brayton, 110 kg for the XRS-style dewar, and 10 kg for the ADR) and will require less than 100 watts of input power. The second system will have a total mass of less than 50 kg (10 kg for the turbo-Brayton, 20 kg for the ADR and 20 kg for the very small cryostat containing the ADR and detectors) and will require less than 150 watts of input power.

6.3 Option 1: Cryocooler, stored liquid helium and sub-Kelvin cooler

Three different coolers could be used to provide the low thermal shield temperature required to extend the lifetime of the liquid helium, namely the miniature turbo-Brayton cooler, the sorption cooler or the 2-stage Stirling cooler. The miniature turbo-Brayton cooler and the sorption cooler are essentially vibration free, but at this time, neither cooler technology has demonstrated continuous cooling at or below 10 K. A technology demonstration is underway for each cooler during 1997.

Turbo-Brayton cooler technology has many excellent features, including essentially vibration free operation, large cooling power per unit mass and volume, high thermodynamic efficiency, and ease of integration. Until recently, only large cooling capacity coolers could be produced due to lack of technology to miniaturize the components for space. A specialized robotic electron discharge milling machine has been commercially developed to produce the miniature turbines required for the compressor and turboalternator for the system. New counterflow heat exchanger designs have also been developed enabling greater efficiency. The high speed compressor turbine, supported by gas bearings, typically rotates at approximately 300,000 RPM. A demonstration shaft and bearings have been on life testing for over 12 years with no degradation in performance. Turbo-Brayton cooler units have been produced that operate at higher temperatures and cooling powers, the challenge for the new system is the redesign of the systems to operate with helium instead of neon as the working fluid and to maintain reasonable efficiencies while working with the non-ideal gas properties of the working fluid.

Sorption cooler technology has made significant progress over the last few years with demonstration of 16K continuous operation and with flight of a 10K periodic sorption cooler, BETSCE. Proposed sorption cooler developmental programs call for operating temperature ranges of 1.5K to 20K with low, 2 to 30 mW, cooling needs while producing negligible vibration and EMI. Good efficiency should be obtainable at these small cooling powers. These systems should prove to be highly reliable due to minimal moving parts, only the valves in the system. A potential drawback to use of this system for HTXS is the need for subcooling of the fluid at approximately 80 to 100K. This subcooling can be obtained by use of another cooler, a Stirling was used for BETSCE, or by radiative cooling if available. It is questionable if a large enough radiative area at an appropriate temperature will be available on HTXS to support use of a sorption cooler.

The 2-stage Stirling can reach 35K and flight prototypes are being life-tested. It may be possible to enhance its performance so 20 K could be achieved. This will be considered as a fall-back option if the newer cooler technologies are not fully developed in time.

A sub-Kelvin cooler is used to provide the required 65 mK for the detectors. There are two sub-Kelvin coolers that could conceivably be used, an ADR or a dilution refrigerator. An ADR, which uses a magnetic cooling cycle, is much more efficient than a dilution refrigerator, but since the heat load from the detectors can be made very small, both can be considered. Dilution refrigerator function by mixing He3 with He4 so there are some fluid management concerns regarding the operation in 0-g. Researchers in Europe are studying an open-cycle dilution refrigerator, where the fluid management is somewhat simpler, for the FIRST mission, and we will keep abreast of the development of this interesting scheme.

The ADR is a relatively mature technology that will be flown on Astro-E. It provides a ro-

bust final cooling stage and its only disadvantage is the requirement for a superconducting magnet. The magnetic field can be shielded but the magnet requires a significant current. The electrical leads for the magnet represent a parasitic heat load on the stored cryogen system. To limit the effect on the stored cryogen, XRS will use superconducting current leads composed of high temperature superconducting materials. The lifetime of the HTXS ADR will be enhanced if an improved version of these superconducting leads can be developed.

The ADR for HTXS will be an advanced version of the one developed to keep the XRS detectors at 65 mK. To decrease the heat load of the ADR on the stored liquid helium, an improved heat switch is required. Four types of heat switches have been considered, an advanced version of the present gas gap heat switch, a magneto resistance heat switch, a mechanical heat switch and a He3/He4 diode heat switch.

The gas gap heat switch has been under development for many years by the Astro-E project. It is unlikely that further breakthroughs can be made with that design. A detailed design for a magneto resistance heat switch has been completed. While the heat switch has a good on/off ratio, it is too fragile to be highly reliable. The mechanical heat switch obviously has the best on/off ratio and will be studied further over the next several years. However, it is a mechanism that has all of the usual failure modes of mechanisms. Therefore, the development of a reliable, cryogenic heat switch will be a difficult undertaking. The He3/He4 diode heat switch has an excellent on/off ratio if the warm end can be operated at 1.2 K or less, as it can on HTXS. It has no moving parts and would therefore be a candidate for a highly reliable heat switch. It is the baseline candidate for the HTXS hybrid cooling system 1. For reasons described below, the mechanical heat switch is the baseline candidate for the hybrid cooling system 2.

The ADR is mounted inside the small superfluid helium dewar which incorporates two vapor cooled shields. The superfluid helium dewar can be made quite small if the heat load from the ADR can be decreased and if the parasitic heat load can be reduced. In addition to the mechanical cooler and ADR heat switch, improved high temperature superconducting wires with low thermal conductivity, high strength, and high reliability are required for the ADR magnet leads and cryogenic valve leads.

A 10 year stored cryogen lifetime is attainable with this design with the ADR heat load on the liquid helium at less than 0.1 mW and with the cryocooler providing a thermal shield temperature of 8 K.

6.3.1 Metrics for the Baseline Cooling System

The proposed cooling system will have a lifetime of at least 5 years with high reliability, a mass of less than 130 kg, an input power of less than 100 watts and a total cost significantly less than the cost of a much more massive design that uses existing technology. The stored cryogen will have a lifetime of 10 years. The sub-Kelvin cooling system will provide the detector array with a stable operating temperature of 65 mK for at least 2 days between recycling. The recycling duration will be less than 2 hours.

6.3.2 Mechanical coolers

A mechanical cooler that provides 10 to 100 mW of cooling at 5 to 10K will be developed. Both the turbo-Brayton and sorption coolers appear to be good candidates for this development. A miniature turbo-Brayton cooler designed to meet the HTXS cooling requirements would require less than 100 W of input power with a radiative cooler heat sink at 300 K, would weigh less than 8 kg and would occupy a volume of less than 1 cubic foot. Preliminary calculations indicate that using this cooler to cool the inner vapor cooled shield to 7 K can reduce the required helium volume from 330 l to less than 50 l and the total mass from 240 kg to less than 120 kg, including the mass of the cooler and ADR. Further mass reduction may be realized if the cooler can be operated immediately before and after launch. The large capacity of the cooler also allows for cooling the outer vapor cooled shield contributing to the volume and mass savings. A comparative study has not yet been performed for the sorption cooler technology. One advantage of these two cooler technologies is that they are inherently vibration-free, in particular compared to the existing Stirling coolers.

6.3.3 Adiabatic Demagnetization Refrigerator

ADR operation and total heat load to the superfluid helium bath can be improved with development of a more efficient heat switch. The development of a diode heat switch has been baselined. It will improve the ADR efficiency and reduce the heat load on the stored cryogen by more than a factor of 2, to less than 0.1 mW, while simultaneously reducing the ADR mass by a factor of 2, to less than 4 kg. The power input to the ADR is set by the electronics operating the ADR. The peak power will be less than 25 watts while the average power will be much smaller.

High temperature superconducting (HTS) wire is presently being developed by industry. A test program on samples obtained from industry is proposed to develop HTS current leads to be used in the dewar for the ADR magnet leads and for valve leads. Low thermal conductivity, strength, and reliability are required. The HTS current leads will provide a current of 1.5 amps to the ADR magnet and cryogenic valves while providing a heat leak of less than 25 microwatts to the stored liquid helium.

6.4 Hybrid Cooling System 2: A Two Stage Mechanical Cooler Design

6.4.1 Technology Requirement

Several proposed astronomy missions including the HTXS system have a desire for long lifetimes ranging from 5 to 10 years or more. To meet these long lifetimes, it is advantageous not to carry stored consumables. The proposed hybrid cooling system 2 is an enhancement to the baseline design where a two stage mechanical cooler system would eliminate the stored liquid helium system. This not only eliminates the stored cryogen but reduces the mass by eliminating the cryogen tank, plumbing system and other hardware associated with a stored cryogen system. This system can be pursued, when the mechanical cooler technology has been proven.

To eliminate the stored cryogen system, the sub-Kelvin cooler must be able to cool from the temperature attained by the cryocooler to the 65 mK operating temperature required

by the detectors. Since all sub-Kelvin coolers function much more efficiently from lower starting temperatures, it is extremely advantageous for the cryocooler to cool to the lowest possible temperature.

Except for magnetic coolers such as ADRs, all cryocoolers use a working fluid as the basis of their thermodynamic cycle. However, the vapor pressure of all working fluids approaches zero as the temperature approaches absolute zero so there is a lower limit on how cold typical cryocoolers can operate. He3 provides the lowest working temperature. A turbo-Brayton cooler using He3 as its working fluid should be able to attain adequate cooling for HTXS at temperatures as low as 3.0 K. Since other cooling cycles require higher working pressure than the turbo-Brayton, no other known cooler (except magnetic coolers) can attain such a low operating temperature at reasonable thermodynamic efficiency. Primarily for that reason, a turbo-Brayton cooler using He3 as its working fluid is the baseline cooler for the hybrid cooling system 2.

We will also investigate in parallel the use of a Stirling cycle cooler coupled to a Joule-Thomson expansion port to reach 4 K. This is a scheme that British Aerospace has been developing for the FIRST mission. The technology and capabilities to develop this cooler exist here in the U.S.

Of the sub-Kelvin cooler alternatives, dilution refrigerators can not function with a heat sink temperature much above 1.0 Kelvin (2.0 K is a reasonable maximum upper temperature). This limitation results from the fact that the dilution refrigerator cools by mixing He3 and He4 and then distilling them in a separate "still". The distilling process will only function if the vapor pressure of the He4 is low compared to the vapor pressure of He3. Above 1 K the vapor pressure of He4 rises rapidly so that the ratio of the vapor pressure of He4 to He3 is no longer a small fraction above about 2 K. Thus, a dilution refrigerator is not an option for the hybrid cooling system 2.

Two realistic options exist for the sub-Kelvin cooler. Both of these options are based on ADR technology. The two ADR approaches are a single stage ADR and a two stage ADR.

The major problem with ADR technology for the HTXS hybrid cooling system 2 is the fact that the magnetic field required to produce appreciable cooling increases as the ADR heat sink temperature increases. For a single stage ADR operating between 3.5K and 0.065 mK the magnetic field used by the ADR will be optimal at about 3.5 tesla. This compares to about 1.5 tesla for an ADR operating between nominally 1.2 K to 65 mK. The increase in the magnetic field will result in a more massive magnet, particularly since the magnetic shielding requirement is increased. Even so, the mass required for the magnet will be much less than the mass of the helium cryogen tank being deleted in hybrid cooling system 2.

The use of a two stage ADR allows the use of two different paramagnetic salts. The lower temperature stage salt can be optimized for the coldest required temperature, namely 65 mK, while the warmer stage can be optimized for higher temperature operation. Typically, Gadolinium Gallium Garnet (GGG) is used for the upper stage. A GGG upper stage can obtain efficient cooling up to a temperature of approximately 8 Kelvin but the magnetic field required is quite large. While the optimal field has not been calculated, typical fields in ADRs based on GGG have been approximately 7 tesla. A field this large results in a massive magnet with significant magnetic shielding requirements. In addition, the most reliable magnets are made with niobium titanium wire than loses much of its current carrying capacity at 7 or 8 K. Therefore, the magnet must be even more massive to produce the

required field (or a less reliable magnet must be used). This massive magnet must be traded off against the increased efficiency of the cryocooler at 8 K versus temperatures as low as 3.5 K. Experience has indicated that this is not likely to be a favorable trade-off.

A better alternative is to operate the GGG stage with a lower heat sink temperature. An optimization of the two-stage ADR has not yet been performed. However, because of the large influence of the mass of the magnet in such an optimization, it is likely that allowing both the upper stage to use a magnet with a much lower field, say 2 tesla, may be a reasonable approximation to an optimal system. After an optimization study is performed on the two stage ADR, a trade off study will be performed to determine the relative merits of using a two-stage ADR versus an single stage ADR. Because of the complexity of the two stage ADR, which must include two sets of magnets, paramagnetic salt pills and heat switches, a single stage ADR will be tentatively baselined for hybrid cooling system 2.

An alternate improved heat switch design is required for hybrid cooling system 2. A He3/He4 diode heat switch will not function at the higher ADR heat sink temperature for cooling system 2. Therefore a gas gap heat switch or a mechanical heat switch must be used. Because of the difficulties encountered with the gas gap heat switch on the XRS project, further development of the heat switch options, either a gas gap heat switch or a mechanical heat switch, is proposed.

6.4.2 Metrics for Baseline Hybrid Cryogenic Cooling System 2

The proposed cooling system will have a lifetime of at least 5 years with high reliability, a mass of less than 50 kg, and an input power of less than 150 watts. There will be no stored cryogen system. The sub-Kelvin cooling system will provide the detector array with a stable operating temperature of 65 mK for at least 2 days between recycling. The recycling duration will be less than 2 hours.

6.4.3 Mechanical cooler

An advanced mechanical cooler that provides 5 to 10 mW of cooling at 3 to 5 K will be developed. This cooler will probably require two stages, with an upper stage cooling a thermal shield at a temperature between the ADR heat sink temperature and the temperature of the radiatively cooled outer shield.

6.4.4 Adiabatic Demagnetization Refrigerator

A system design of the ADR for the HTXS hybrid cooling system 2 has not yet been completed. Preliminary estimates show a mass of less than 20 kg. The power requirement will be set by the electronics to operate the ADR and will be less than 30 watts peak. The average power is quite low.

6.5 Mission criticality

The development of a 3–5 K mechanical cooler system is critical to meet the weight, volume and lifetime requirements of the mission. This technology is also critical to several other

future NASA programs. The development of this technology is well underway and significant advances are expected over the coming year.

6.6 Milestones for the Cryocooler Development

| Milestones | Date |
|---|-------|
| ----- | |
| Mechanical Cooler: | |
| Technology demonstration of 5 - 10 K cooler | 12/97 |
| Design 5 - 10 K engineering model cooler | 6/98 |
| Complete component development | 12/98 |
| Complete fabrication of engineering model | 9/99 |
| Complete technology validation of 5 - 10 K cooler | 12/99 |
| Note: the first engineering model cooler to be fabricated is a single stage unit. The current proposal for HTXS is a two-stage unit. If a demo unit of the proposed cooler is required by the year 2000, an additional unit can be fabricated and tested concurrently with the single stage unit. | |
| Complete system trade-off study for HTXS hybrid cooling system #2 | 3/98 |
| Technology demonstration of 3 - 5 K cooler | 12/99 |
| Design 3 - 5 K engineering model cooler | 6/00 |
| Complete component development | 12/00 |
| Complete fabrication of 3 - 5 K engineering model | 9/01 |
| Complete technology validation of 3 - 5 K cooler | 12/01 |
| ----- | |
| Sorption Cooler: | |
| Prove compressor life | 97 |
| Prove low cooling power scaling | 97 |
| Fly 25K cooler on UCSB LDB | 12/97 |
| Develop flight-like 20K cooler | 98 |
| Characterize/quantify 20K cooler | 99 |
| Complete 6-8K cooler detail design | 99 |
| 20K cooler for TESRE for ground science validation | 00 |
| Develop 6-8K cooler | 00 |
| Characterize/quantify 6-8K cooler | 01 |
| ----- | |
| ADR Heat Switch: | |
| Perform trade-off analysis on heat switch #1 | 9/97 |
| Complete design of diode heat switch | 3/98 |

| | |
|---|-------|
| Fabricate and thermal test tech demo of heat switch | 12/98 |
| Fab and test eng. model diode heat switch | 12/99 |
| Perform trade-off analysis on heat switch for hybrid cooling system #2 | 6/00 |
| Complete design of heat switch #2 | 12/00 |
| Fabricate and thermal test tech demo of heat switch | 12/01 |
| Fab and test eng. model heat switch | 12/02 |

ADR with 3 to 5 K heat sink:

| | |
|---|-------|
| Perform trade-off analysis on ADR for hybrid cooling system #2 | 12/98 |
| Complete design ADR for system #2 | 6/99 |
| Fabricate and test tech demo model ADR | 12/00 |
| Fab and test engineering model ADR | 12/01 |

High temperature current lead:

| | |
|---|------------|
| Follow industry development of high Tc wire | Continuous |
| Procure and functional test wire samples | Continuous |
| Fabricate current leads to HTXS specs | 12/98 |
| Qualification test current leads | 12/99 |

7 Hard X-ray telescope (HXT)

In this section, we present the overall requirements and specifications for the HTXS HXT, and the status and required technology development for the HXT optics and focal plane. In order to set a context for the technology requirements, we first review the general approaches to achieving the desired performance, and illustrate these with specific designs utilizing technological parameters which appear feasible within the timeframe set in our technology development plan. In the context of these example designs, we discuss the scaling of the telescope performance with the critical design parameters, and also how the designs may be extrapolated to achieve enhanced sensitivity at high energies. In the final portion, we review the current state of optics, multilayer and detector technologies applicable to the HXT, define the required technology development, and present a schedule and budget for this effort.

7.1 Requirements for the HXT

The performance requirements for the HTXS HXT are summarized in Table 1. The baseline requirements, listed at the top of Table 1, are derived from the primary science objectives of the HTXS mission. In addition, several performance enhancements over this baseline are desirable, and would expand the range of possible scientific investigations. These are also listed, in priority order, in the bottom section of the table.

| Baseline HXT Requirements | |
|------------------------------------|--|
| Effective Area | $\geq 1500 \text{ cm}^2$, 6 – 40 keV |
| Signal to Background Ratio | > 1 for $T_{obs} \lesssim 2 \times 10^4 \text{ s}$ |
| Field of View | $\geq 8'$ ($E < 25 \text{ keV}$) |
| HPD | $\geq 4 \times \text{HPD}$ ($E > 25 \text{ keV}$) |
| $\Delta E/E$ | $\lesssim 1'$ |
| | $\leq 10\%$ at 40 keV |
| Desirable Performance Enhancements | |
| Signal to Noise | > 1 for $T_{obs} \lesssim 10^5 \text{ s}$ |
| Effective Area | $\geq 800 \text{ cm}^2$ 40 – 80 keV |
| HPD | $\lesssim 30''$ |
| Field of View | $> 10'$ ($E < 40 \text{ keV}$) |
| $\Delta E/E$ | $\leq 5\%$ at 40 keV |

Table 1: Performance requirements for the HXT. Also shown are desirable enhancements, in order of priority, which set additional technical goals for the instrument.

The mechanical envelope available to the HXT on each of the six satellites limits the total weight (per satellite) to $\lesssim 130 \text{ kg}$, the geometric aperture for the mirrors to $\lesssim 0.5 \text{ m}^2$, and the focal length to be between 8 and 12 meters.

Several options are being considered for the HXT optics and detectors. Those combinations which demonstrate they can achieve the above requirements will be considered for final implementation. The design with the best performance, weighted with the above priorities, which does not exceed the weight, size or cost envelope will be chosen for implementation.

7.2 Background: Technical Approach to Hard X-ray Focusing

The sensitivity and signal-to-background requirements for the HXT require focusing, or concentrating of the signal (*ie.* ratios of collecting area, A_{coll} , to effective detector area, A_{det} significantly greater than unity). Due to limitations on the achievable detector background, collimated or coded-aperture systems cannot approach the necessary sensitivity within the available envelope.

The familiar technical challenge to extending traditional grazing incidence optics into the hard X-ray band ($E > 10$ keV) is the decrease with energy in graze angle for which significant reflectivity can be achieved. For a Wolter or conical approximation mirror geometry, the graze angle, γ , on a given mirror shell is related to the focal ratio by $\gamma = 1/4 \times (r/f)$, where r is the shell radius and f is the focal length. If one maintains this geometry, two approaches to extending mirror reflectivity to high energy are possible:

1. utilize small focal ratios (r/f). By using multiple telescope modules of small radius in a highly-nested geometry, low graze-angle telescopes can be designed, using standard metal reflective coatings, which extend the effective area to the requisite energy, or even higher.
2. increase, for a given r/f , the graze angle for which significant reflectivity can be achieved. Coating the reflective surfaces with multilayer structures, which operate on the principal of Bragg reflection, can substantially increase the maximum graze angle for which significant reflectivity is achieved over a relatively broad energy range.

For practical designs based on either approach the focal ratios are smaller than for conventional grazing incidence telescopes operating in the soft X-ray band. In the first case, special coatings on the optics are not required, and for a fixed focal length, multiple telescopes of small diameter are used. For the second case, multilayer reflective coatings consisting of many (20 – 600) layers are deposited on the optics, and mirror shells with larger graze angles can be employed, increasing the outer mirror radius, field of view (FOV), and decreasing the required number of modules. For the multilayer telescopes, as graze angles increase above the critical angle and the multilayer coatings become effective, the reflectivity of the mirror surfaces drops, and for a fixed collecting area more mirror surface area is required compared to low graze angle telescope designs.

Other concentrating techniques and mirror geometries such as polycapillary optics, Microchannel Plate (MCP) optics and Kirkpatrick-Baez telescopes can also be extended into the hard X-ray band, however given the current state of technology and the desire for good imaging performance (small HPD and large concentration factor) we currently consider systems based on Wolter-I or conical optics to be the most attractive. It should be noted that a significant effort to develop MCP optics is being pursued by the European Space Agency (ESA), and as technology develops, this option may become competitive in the future.

7.3 Example Telescope Designs

In the following sections, we discuss specific designs for the HXT which utilize technological parameters which appear feasible in the near future. We present calculations for a telescope

designed with a high-energy cutoff between 40 and 50 keV, and show how the design scales with telescope focal length. We also show how this design can be extrapolated to achieve collecting area extending to higher energy. Finally, we present an example of a low-graze angle design which does not employ multilayer coatings.

7.3.1 Graded Multilayer Telescope Design

Graded multilayers operate on the principle of Bragg reflection. Traditional multilayers are produced by manufacturing alternating layers of high and low index of refraction materials of a given thickness on the surface of an optic, and are effective over a narrow energy band. By slowly varying, or grading the d-spacing (thickness of the layer pairs) throughout the multilayer, enhanced reflectivity can be achieved for a range of X-ray energies at incidence angles significantly above the critical angle. Figure 1 shows a comparison of X-ray reflectivity as a function of incidence angle at 45 keV for a W/Si multilayer coating compared to a conventional metal coating, illustrating the larger graze angles which can be employed for multilayer hard X-ray telescopes.

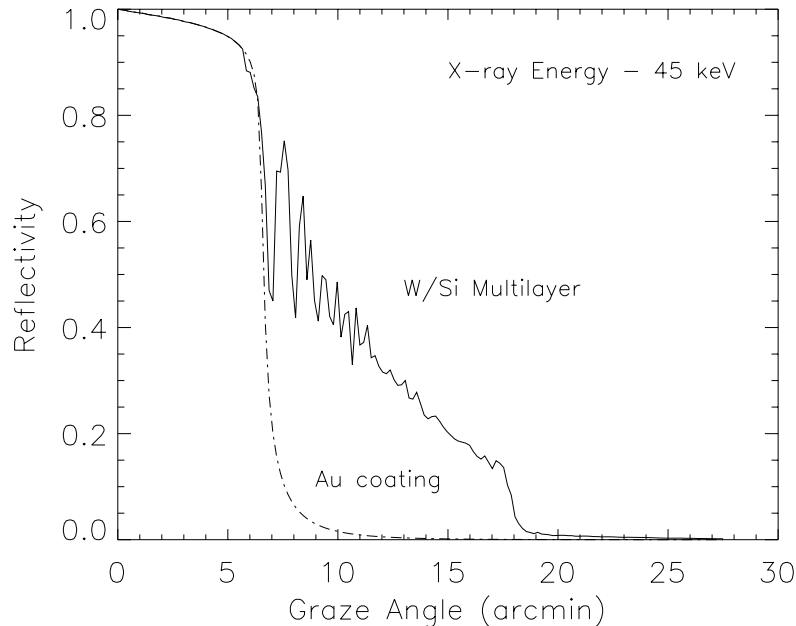


Figure 1: Comparison of X-ray reflectivity as a function of incidence angle at 45 keV for a W/Si multilayer coating, compared to a conventional metal coating. This illustrates the larger graze angles which can be employed for multilayer hard X-ray telescopes.

The requirements for the multilayer materials are that the K absorption edges not lie in the energy range of interest (10 – 50 keV), and that the two materials employed be chemically compatible for forming stable thin films. This is satisfied by several material combinations that have been used to fabricate X-ray multilayers with the appropriate dimensions. The most promising combinations for the HXT include W/Si (W K-edge at 69.5 keV), Ni/C (both edges below 10 keV), and Pt/C (Pt K-edge at 78.4 keV). Practical limits on the multilayer parameters are d-spacings between 25 Å and 100 Å, number of layer pairs less

than 500, and total coating thicknesses below $\sim 2 \mu\text{m}$. Technical complexity and coating time increase as a relatively steep function of total coating thickness and number of layers. Achievable interfacial surface roughnesses range from $4.5 \text{ \AA} - 5.5 \text{ \AA}$.

The first design we discuss has a high-energy cutoff between 45 and 50 keV, and satisfies the basic HTXS performance requirements. For this example design, we use W/Si multilayers, since they have been fabricated with low interfacial roughness of 4.5 \AA , and the materials are relatively inexpensive. Table 2 gives the design parameters as a function of mirror shell radius for a telescope of focal length 8.5 m. The multilayer layer pair thicknesses follow an exponential spacing for the form given in Joensen, 1995 (PhD thesis, University of Copenhagen). The minimum d-spacing is dependent on shell radius (or graze angle), and is indicated in the table. The maximum d-spacing is 200 \AA . As the graze angle on the shells increases (*ie.* as the shell radius increases), a smaller minimum d-spacing is required to achieve the same upper-energy cutoff. The number of layer pairs and total coating thickness also increase with shell radius, because as the graze angle increases, the multilayers must be effective over a larger energy range. For the smallest mirror shells, which have graze angles below the critical angle at 45 keV, we use Iridium metal coatings.

| shell radius (cm) | graze angle ($^{\circ}$) | material | d_{min} (Å) | # of layer pairs | thickness (μm) | # of shells |
|----------------------|-------------------------------|----------|---------------|---------------------|--------------------------------|-------------|
| 3.0 – 5.5 | 3.1 - 5.6 | Ir | – | – | – | 37 |
| 5.5 – 6.9 | 5.6 - 7.0 | W/Si | 58 | 15 | .123 | 18 |
| 6.9 – 8.3 | 7.0 - 8.4 | W/Si | 48 | 25 | .170 | 16 |
| 8.3 – 9.7 | 8.4 - 9.8 | W/Si | 40 | 40 | .225 | 14 |
| 9.7 – 11.1 | 9.8 - 11.2 | W/Si | 34 | 60 | .287 | 12 |
| 11.1 - 12.5 | 11.2 - 12.6 | W/Si | 30 | 120 | .50 | 11 |
| 12.5 – 14.0 | 12.6 - 14.2 | W/Si | 27 | 140 | .526 | 11 |

Table 2: Design parameters for a multilayer telescope designed to have a upper energy cutoff between 45 and 50 keV.

The inner mirror shell radius is determined both by technical limits on the minimum shell radius that can be manufactured, and by the diminishing area per shell obtained as the radius gets small. The outer mirror shell radius is determined by the multilayer reflectivity. After some point, as the number of layers increases, the reflectivity decreases, and little additional area is gained. At some radius achieving high-energy reflectivity requires d-spacings smaller than the technical limit set by manufacturing considerations.

Using reasonable extrapolations of current technologies, this design can be implemented within the HTXS mission envelope. To achieve the desired effective area we require three mirror modules on each satellite. Figure 2 shows the total effective area for the six satellites, assuming an interfacial roughness for the multilayers of 4.5 \AA . Although several technologies are being considered for the mirror shells and detectors, we illustrate the viability of the multilayer approach by considering a specific implementation which employs foil mirrors and room-temperature solid state CdZnTe detectors. Table 3 shows the basic instrument parameters, illustrating that this implementation does not exceed the allowed mechanical envelope. The mirror parameters (achievable foil thicknesses and dimensions) are scaled from the SODART foil telescopes, and are therefore technically reasonable.

To calculate the instrument sensitivity and signal to background ratio we must assume a

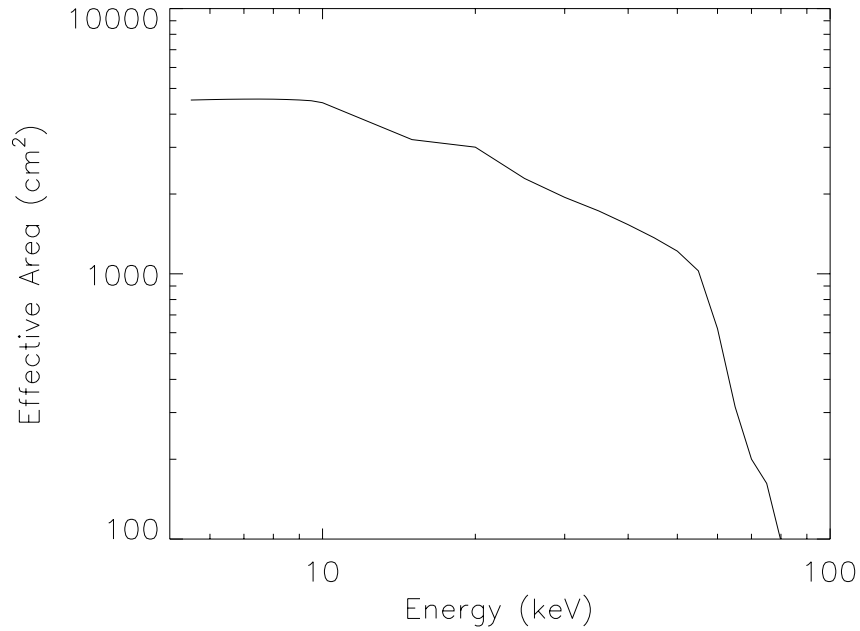


Figure 2: Effective area as a function of area for the telescope designed with a high-energy cutoff between 45 – 50 keV. The interfacial roughness on them multilayers is 4.5\AA .

| | |
|-----------------------------|-------------------------------|
| number of modules/satellite | 3 |
| Mirror shells | Al foil 0.3 mm – 0.5 mm thick |
| Detector | CdZnTe |
| Shielding | 2 cm BGO |
| Mirror mass | 98 kg |
| Focal plane mass | 28 kg |
| Geometric aperture | 0.32 m^2 |

Table 3: Example instrument parameters.

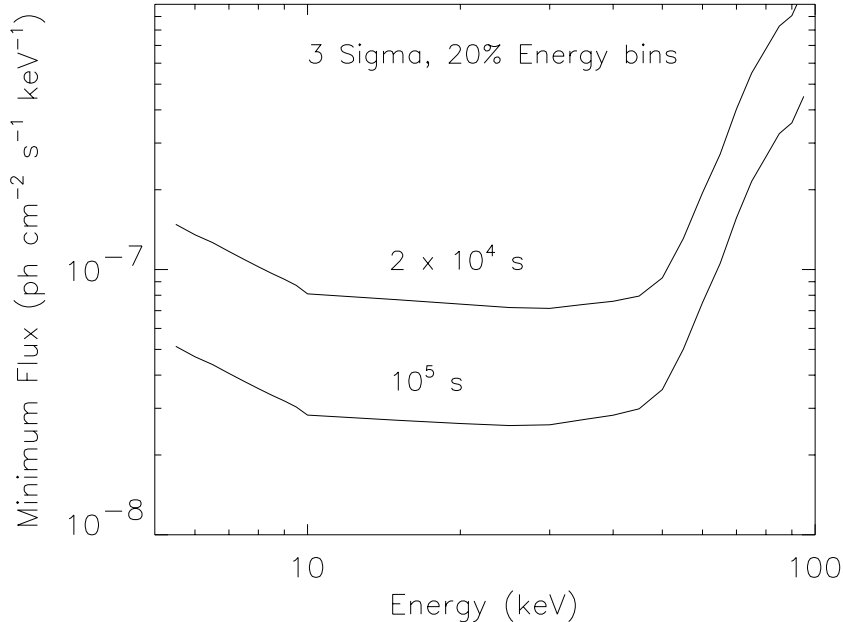


Figure 3: Continuum sensitivity for 2×10^4 and 10^5 second observations for energy bandwidth of 20%.

HPD for the telescope and internal background level for the detectors. Based on extrapolations of current mirror technologies, a HPD of $1'$ for the mirrors is a reasonable goal. To be signal limited for observation times of 2×10^4 s requires an internal detector background level of $< 10^{-4}$ cts $\text{cm}^{-2} \text{s keV}^{-1}$. To achieve this background rate requires careful focal plane design and active shielding at the level indicated in Table 3. Figure 3 shows the three sigma continuum sensitivity for an energy bandwidth of 20% ($\Delta E/E = 0.2$). For comparison, the continuum sensitivity levels indicated in Figure 3 represent a factor ~ 100 improvement over the HEXTE experiment on *XTE*.

Scaling of Design Parameters with Focal Length

Since the telescope focal length, f , is an important parameter which also affects the design of the soft X-ray telescope, it is interesting to consider how the HXT telescope performance and envelope scale with focal length. If all mirror parameters (*ie.* outer radius, inner radius, length, etc.) are scaled proportionally with f , the same effective area and concentration factor are achieved, independent of focal length by scaling the number of telescope modules like $N_{mod} \propto 1/f^2$. This is because the effective area per module scales as the square of the outer mirror radius. The spotsize on the detector increases as f^2 , so although longer focal length implies fewer modules, it does not translate into better concentration factor. Since the dimensions of an individual mirror and detector also increase approximately as f^2 , the total instrument mass is also roughly independent of f .

As the focal length decreases, however, technical limitations prohibit direct scaling of the mirror shell parameters with f (for example there is a minimum inner shell radius and shell thickness that can reasonably be achieved). Due to these obscuration factors, which are roughly constant with f , for focal lengths below 5 – 6 m the aperture is less effectively

| f | # modules | A_{eff} (40 keV) (cm ²) | shells/module | outer diameter (cm) | mirror mass (kg) | focal plane mass (kg) |
|------|-----------|--|---------------|------------------------|---------------------|--------------------------|
| 8.5 | 3 | 1532 | 119 | 28 | 98 | 28 |
| 10.5 | 2 | 1504 | 141 | 35 | 101 | 25 |
| 14.5 | 1 | 1513 | 198 | 48 | 103 | 21 |

Table 4: Scaling of instrument parameters with focal length.

utilized, and the collecting area per unit mass is a sharply decreasing function of f . Table 4 shows how the basic telescope design described above scales with increased focal length. It can be seen that the total telescope mass, effective area, and concentration factor remain roughly constant as f increases, while the number of modules decreases. As the focal length increases, and the number of mirror modules decreases, the focal plane is somewhat easier to instrument, however it will likely be more difficult to maintain figure for the larger-diameter mirror shells.

Extending Multilayer Designs to Higher Energy

We briefly consider how the effective area can be extended to energies higher than 50 keV. By decreasing the minimum multilayer d-spacing for fixed graze angle, the mirror reflectivity can be extended to higher energy. This requires, however, a significantly increased number of layer pairs and total multilayer coating thickness. Obtaining significant collecting area at high energy usually also involves decreasing the average graze angle for a module by decreasing the outer mirror diameter (for fixed focal length), thus increasing the number of detector modules and decreasing the concentration factor at lower energy. Depending on the desired upper energy cutoff and specific design, some performance at lower energies is usually sacrificed.

| Cutoff at 78.4 keV | |
|--|---------------------|
| multilayer material | Pt/C |
| maximum # layer pairs (outer shell) | 200 |
| maximum coating thickness (outer shell) | 0.7 μm |
| # modules | 4 |
| outer mirror radius | 11.5 cm |
| mirror + focal plane mass | 116 kg |
| geometric aperture | 0.35 m ² |
| collecting area/effective detector area (40 keV) | 945 |
| Cutoff at 100 keV | |
| multilayer material | Ni/C |
| maximum # layer pairs (outer shell) | 600 |
| maximum coating thickness (outer shell) | 1.4 μm |
| # modules | 6 |
| outer mirror radius | 9.5 cm |
| mirror + focal plane mass | 126 kg |
| geometric aperture | 0.35 m ² |
| collecting area/effective detector area (40 keV) | 630 |

Table 5: Parameters for multilayer telescopes designed to cut off at 78.4 and 100 keV.

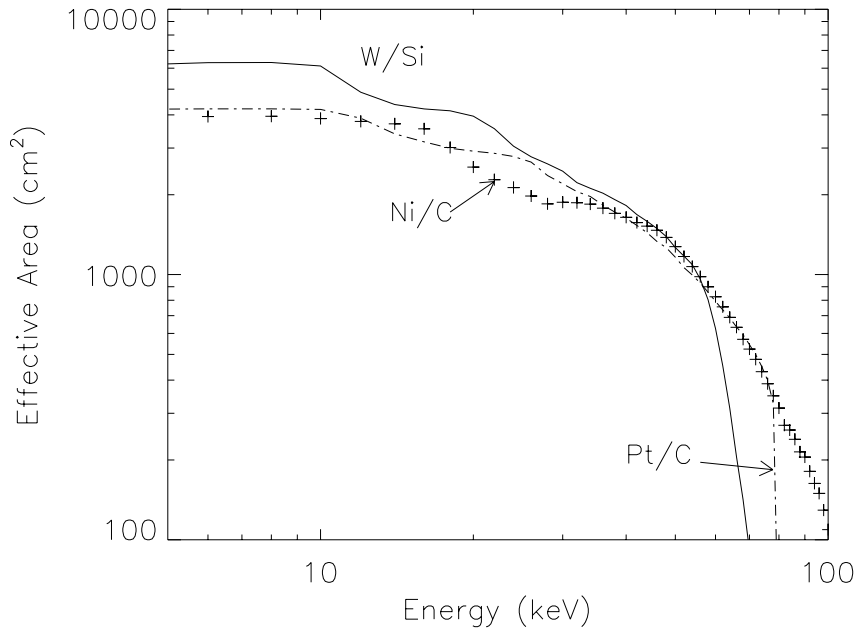


Figure 4: Effective areas for telescope designs with high energy cutoffs at 50, 78.4 and 100 keV.

| | | | |
|-------------------------|-----|-------------------------|-----------------------|
| inner shell radius (cm) | 2.5 | shell substrates | ribbed electroform Ni |
| outer shell radius (cm) | 5.8 | mirror mass | 98 kg |
| shell length (cm) | 43 | effective area (20 keV) | 1565 |
| shells/module | 65 | effective area (40 keV) | 1501 |
| modules/satellite | 8 | FOV (arcmin) (20 keV) | 5' |

Table 6: Parameters for a low-graze angle telescope employing traditional metal coatings.

Table 5 shows the basic parameters for telescope designs extended to 78.4 (Pt K-edge) and 100 keV. Figure 4 compares the effective areas for the 50 keV cutoff described above and these two designs.

7.3.2 Low Graze Angle Telescope

It is possible to avoid the use of multilayers altogether by decreasing the average graze angle on the mirrors. This can be accomplished by reducing the outer mirror diameter, achieving the same collecting area by increasing the number of mirror modules. Table 6 shows the basic telescope parameters for a low graze angle telescope designed to cutoff at 50 keV. With eight modules per satellite, equivalent collecting area can be achieved at 40 – 50 keV to the multilayer designs described above. Due to the small radii and long shells required for this design, replicated shells are a more promising technical approach than foil mirrors, which are more difficult to fabricate with small radius. The mirror weights have therefore been calculated using thin ribbed electroform Nickel shells.

For the same mirror HPD, the low graze angle telescope has a smaller ratio of collecting area to effective detector area ($A_{coll}/A_{det} = 473$ for a HPD of $1'$) than the multilayer telescope with equivalent high-energy cutoff described above. Due to the smaller average radii, however, it is likely that an HPD significantly less than $1'$ can be achieved for such a design, and thus a concentration factor similar to, or better than that specified above for the multilayer telescope could be realized. In addition, it should be noted that if light replicated substrates of the type being developed for the SXT become available, a significant weight advantage could also be achieved for this design over the multilayer telescopes.

7.4 Technology Status and Development Requirements

In this section, we describe the technology status and development requirements for the HXT. We will concentrate our efforts on a primary approach, which has the highest probability of achieving the baseline mission requirements. In addition, we identify enhancing technologies which, if developed, would allow us to significantly reduce the mass envelope and/or improve the performance of the mission over the baseline requirements.

7.4.1 Hard X-ray Optics

Primary Approach

The requirements listed in Section 7.1 above determine the minimum mirror effective area and HPD for the HXT mirrors. These must be achieved for a total mirror mass ≤ 100 kg and a geometric aperture < 0.5 m².

The primary technology for the HXT substrates is to fabricate segmented shells in a conical approximation to a Wolter-I geometry. This approach is directly derived from the foil mirrors developed for *ASCA* and *Astro-E*. A HPD of $3'$ was achieved for the *ASCA* mirrors, and approximately $1'$ is projected for the *Astro-E* mirrors. For the HXT, the shells could be fabricated from Epoxy-Replicated-Foils (ERF), as is being done for *Astro-E*, or from thermally-formed glass substrates. Both of these substrates are capable of meeting the mass requirement of 100 kg for the HXT optics. The ERFs have the advantage of flight heritage from *Astro-E*, and the glass substrates have the advantage of lower surface roughness (4\AA rms as opposed to 5\AA for ERF) and ease of coating. The reflectivity of the multilayer depends strongly on the surface roughness between the layers, and achieving low values is dependent on the smoothness of the initial substrate. In either the case of foils or glass, the approach draws strongly from a flight-proven technology.

In order to insure that $\leq 1'$ is achieved for the HXT mirrors, development is required to determine the level at which any stress in the multilayer film affects the optic. Preliminary characterizations of the thin-film stress combined with analytic work indicate that distortions will be at an acceptable level. Improvements and modifications in foil mounting and alignment may be required, and analytic work to determine the total error budget for the HXT optics is necessary. It is important to note that the HXT signal to background ratio is strongly dependent (like the square) on the mirror HPD. Any improvements in the HPD will therefore greatly reduce the requirements on the detector background. This can be translated into reduced shielding mass and improved scientific performance. The improvements in resolution being pursued for the SXT segmented mirrors are therefore important

for the HXT as well.

The best approach to fabricating the multilayer coatings for the HXT is by magnetron sputtering. One major advantage of a segmented optic is that it can be coated using conventional planar magnetron sputtering systems. This technique has been used to coat both curved glass and ERF substrates with adequate uniformity and quality. In the case of glass shells, W/Si graded multilayers of a design very similar to those which would be used with the HXT were deposited. For the ERF, a single d-spacing multilayer was deposited, and good uniformity across the segment demonstrated. However, only a small number of shells have been coated, and further work is necessary to demonstrate consistent reflectivity, especially in coating chambers which have configurations capable of mass-production. The multilayer reflectivity is a strong function of the interfacial roughness, and improvements in deposition technologies and short length-scale substrate smoothness will result in significantly reduced substrate area requirements, reducing both weight and cost, and therefore enhancing performance. Efforts to minimize both substrate and multilayer interfacial roughness should be given high priority. Finally, the HXT requires coating of a large number (up to 20,000 segments) of optics, and deposition facilities capable of reliably coating and characterizing this quantity must be designed.

In summary, the most critical development items for the HXT primary optics are:

- verification of HPD through demonstration of prototype optics and mounting.
- minimization of surface roughness of substrates.
- characterization and minimization of stresses in graded multilayer films.
- development of processes for uniform coating onto curved, open substrates capable of being implemented in a mass production system.
- optimization of coating process to achieve minimum interfacial roughness for candidate multilayer materials in systems capable of mass production (i.e., capable of high deposition rates).
- design and demonstration of mass production coating facilities.

Optics Technology Enhancements

Significant performance enhancement for the HXT would be achieved by reducing the mirror HPD. Optics replicated as complete shells have demonstrated significantly improved resolution over segmented optics. The JET-X replica optics have achieved 20'' HPD compared to 3' for the ASCA and SODART (on Spectrum X-Gamma) foil telescopes or the 1' projected for *Astro-E*. This corresponds to more than an order of magnitude (a factor 100 for ASCA and SODART) less pixel area, and correspondingly lower background at the focal plane. The primary disadvantage of closed shells is the high mass of the Ni from which the substrates are made. Given the less-stringent resolution requirement of the HXT, segmented optics have therefore been chosen as the highest-priority for development. Lightweight closed-shell optics are, however, being developed for the HTXS SXT. Should these be demonstrated, the application of replicated closed shells for the HXT will be re-evaluated.

One advantage of replicated closed shells for multilayer telescopes is that they are intrinsically less subject to distortions from multilayer stress due to their closed geometry. The

axial loads due to the multilayers are even, and should not result in figure distortion. Replicated shells are therefore more likely to achieve angular resolution significantly better than the baseline requirement. In addition to the potential angular resolution advantage, the handling and final assembly of closed shell replicated optics is simpler than for segmented optics, which typically have eight segments per mirror shell which must be mounted and aligned. Although complex multilayers have been deposited on Nickel replica substrates, the reflectivity was compromised due to increased microroughness of the replicas. Ongoing efforts to reduce the substrate roughness are important. Closed shells are more difficult to coat, as the geometry of standard sputtering systems does not easily accommodate coating on interior surfaces. Closed shells of significantly larger diameter than those required for the HXT have been coated using standard deposition techniques for the AXAF optics, and although scaling considerations indicate that it is possible, it must be demonstrated that multilayers can be deposited using similar technology on smaller diameter shells. The constant target-substrate distance necessary for good quality coatings is more difficult to achieve with a closed cylindrical geometry. However, a difference in diameter of 15 inches was achieved for AXAF, and the proposed geometry for the HXT would involve similar differences in shell geometry. The weight of the replicated optics is still the biggest disadvantage, and the principal reason for choosing segmented optics.

Another option which could offer significant advantages for the HXT is a low graze-angle telescope design which does not employ multilayers. Given the small radius (2 – 6 cm) and length (25 cm) of the optics employed in these designs, the shells must be fabricated as closed units by replication. The advantage of this approach is that the reflectivity of the surfaces below the graze angle is large, and therefore less substrate area is required in order to achieve the same effective area. Given the mass of current replica optics, the potential advantage is not achieved. If, however, light-weight replica optics are produced for the SXT that can be extrapolated to small radius optics, the use of a low graze angle telescope could offer significant advantages in mass and also angular resolution.

Finally, ESA is making significant investment in development of MCP optics. Although these have the inherent disadvantage of requiring more mirrors (and hence lower concentration factors), thus also requiring a large area detector or a large array of small detectors, if a breakthrough in performance is achieved, these could offer some mass savings. Given ESA's technology investment, and the possibility of a technical breakthrough which would make this option attractive, we will continue to monitor progress on this effort, and consider it as a possible technology.

7.4.2 HXT Detectors

Primary Detector Option

For the 8.5 m HTXS focal length, the required detector spatial resolution is $\sim 500\mu\text{m}$, and the minimum detector size to cover an $8'$ FOV is 1 cm. The background required in order to achieve the baseline signal to noise is 1.0×10^{-4} cts $\text{cm}^{-2}\text{s}^{-1}\text{keV}^{-1}$ for a $1'$ telescope HPD. For energy resolution, the primary science goal of studying continuum emission in point-like sources dictates a rather modest resolution of 10% FWHM at 40 keV.

The primary detector option is a CdZnTe solid state pixel detector coupled to a custom VLSI readout. CdZnTe can achieve the required spatial and energy resolution in a compact,

light-weight package which minimizes the mass in the active shield. Because of its wide band gap, CdZnTe does not require cryogenic systems, and can achieve good noise performance over a range of temperatures from -40° C to 25° C. Individual pixel arrays developed for medical imaging have been demonstrated, and achieve the HXT requirements.

CdZnTe is a relatively-recently developed, and significant effort must be put into design of readouts capable of achieving less than 100 electrons rms noise levels, robust space-qualified techniques for packaging and bonding of the detector and readout, and device optimization and characterization. This should include detailed studies of materials properties, and determination of the factors limiting the device performance.

Another technology which has been demonstrated to achieve the HXT requirements is Xenon microstrip detectors. These have been demonstrated and packaged for balloon flight applications. Because the geometry is less compact, and the quantum efficiency at high energies lower than the CdZnTe, these detectors are somewhat less attractive. However, they have demonstrated the required noise performance and low-energy threshold. We therefore consider them competitive. Since the development of microstrip detectors is more advanced, we place a higher priority on addressing the technical issues associated with the CdZnTe.

For any detector technology, background is a critical issue. The low signal to background ratio is one of the most critical scientific goals of the HXT. The level of 1.0×10^{-4} cts $\text{cm}^{-2}\text{s}^{-1}\text{keV}^{-1}$ is 1/3 of the HEAO A-4 LED background level. While calculations indicate that this is feasible with careful shielding design, it is essential to verify the model calculations with data from balloons and satellites. In addition, advanced shielding options should be considered to further reduce levels.

Enhancing Technologies

Solid state pixel and strip detectors fabricated from Germanium could potentially provide improved energy resolution over the primary detector options. These detectors are extremely attractive, and could be especially interesting if the energy band of the telescope extends to higher energies, where the nuclear lines from ^{44}Ti (68, 78 keV) in supernova remnants lie. They do, however, require significant technology development in order to be viable. In addition, Ge detectors require stable operating temperatures around 85 K, placing restrictions on the spacecraft design, and possibly requiring a cryogenic system. Since the primary science goals of HTXS do not extend the energy response into this band, we do not invest in Ge detectors for a primary option. We will, however, continue to monitor the progress of this development, and re-evaluate it should significant progress occur independently.

7.4.3 Milestones for the HXT Development

HXT Optics

| Milestone | Date |
|--|------|
| MULTILAYER MIRRORS: | |
| Coating and figure characterization - single quadrant/foil | 1997 |
| Multilayer stress and reflectivity characterization | 1997 |
| Coating/characterization single closed shell | 1998 |
| Design/material choice optimization | 1998 |
| Mounting and characterization subset of shells | 1998 |
| Prototype demonstration | 1999 |

| | |
|---|------|
| Final telescope design and substrate choice | 2000 |
|---|------|

HXT Detectors

| Milestone | Date |
|--|------|
| CdZnTe DETECTORS: | |
| Pixel detector with 0.5 mm demonstrated with readout | 1999 |
| GAS MICROSTRIP DETECTORS: | |
| Flight-quality Xe gas microstrip detector with 0.5 mm spatial resolution at 40 keV | 1999 |

| | |
|---------------------------|------|
| Final detector and shield | 1999 |
|---------------------------|------|

ELECTRONICS:

| | |
|---|------|
| Rad-hard ASIC multiplexer chips developed with < 100 electron noise per channel | 2000 |
| Flight-quality interconnect technology between detectors and ASICs proven | 1999 |

SHIELDS AND SIMULATIONS:

| | |
|--|------|
| Complete background model for HTXS orbit | 1998 |
| Shield design achieving required background | 1998 |
| Balloon flight demonstration of shield/model | 1999 |

| | |
|-------------------------------|------|
| Detector system flight design | 2000 |
|-------------------------------|------|

| | |
|---|------|
| Prototype of detector system demonstrated | 2000 |
|---|------|

8 Extendible Optical Bench (EOB)

8.1 Introduction

The Extendible Optical Bench (EOB) is an integrated system that provides all of the structural, mechanical, electrical and thermal interface accommodations for all of the HTXS instruments. The EOB consists of:

1. A thermally and structurally stable deployable structure that provides the separation distance, or focal length of at least 8m between the instruments' optical assemblies and their respective detector and electronics package assemblies;
2. Instrument mounting systems including precision remote controlled electro-mechanical alignment devices as required by trade analysis between design, or adjust for controlling alignments;
3. Thermal control systems that maintain the optics and detector assemblies at their designated temperatures;
4. Deployable signal and power cables that interconnect the elements of the mirror platform assembly with the detector platform assembly; and
5. A deployable scattered light shield that prevents stray light from entering the SXT light path.

8.2 Current Status

No known deployable structures exist that are capable of supporting more than 400 kg at 8 meters and meet the long term precision pointing stability requirements of the HTXS mission. While several deployable structural systems have been developed and successfully flown in the past, their ability to support heavy masses and meet the ~ 5 arc second position stability requirement over long periods of time has not been ascertained.

In conjunction with the successful development of a deployable structure, a precision remote controlled adjustment system may be necessary to correct for possible misalignments caused by deployment, thermal instability and aging. While no known systems currently exist, sensors and actuators essential to providing the necessary precision control are presently within the state of the art.

Thermal design of the EOB can proceed using standard engineering practices. Techniques for the design of mechanical systems to deploy interconnecting cables, and the light shield are also within the state of the art.

8.3 Success Criteria

Success criteria for the development of the deployable structure are as follows:

1. Demonstrate that an engineering model of the proposed structure can be deployed in a 1 "g" field (using g negation techniques) and meet all precision positioning requirements in an on orbit simulated thermal environment;

2. Demonstrate that an engineering model of the most sensitive alignment system can meet the pointing and stability requirements in an on orbit simulated thermal environment; and
3. Show that an engineering model of the proposed cable and light shield mechanisms can both meet the requirements in a room temperature test.

8.4 Technology Requirements

The deployable structure must be capable of

1. Positioning the SXT and HXT optics at their specified focal length and
2. Position these units to within the dynamic range (approximately 2 degrees), of the adjustment and alignment mechanisms. The stability of the structural assembly must be within 5 arc seconds for time periods of up to 100 hours The EOB launch configuration must fit within the launch vehicle fairing, be compatible with the spacecraft configuration and weigh no more than 100 kg.

The bench design or the alignment system must be capable of

1. Preventing or accommodating an initial (post launch) offset of 2 degrees,
2. Position the instruments' optical systems and their respective detector assemblies to within 5 arc seconds of the calibration X-ray target source, and
3. Maintain this alignment for 100 hours.

8.5 Metrics

Successful testing of an engineering model of the EOB deployable structure is the primary milestone for the development of the EOB system.

8.6 Mission Criticality

The EOB deployable structure is critical to the HTXS mission. Unless this system is successfully developed, the mission objectives cannot be met.

8.7 Deployable Structures

The following options will be studied.

8.7.1 Telescoping Tubes

Preliminary design studies reveal that a 3 stage telescoping graphite epoxy tube system is a feasible approach. Graphite epoxy is the material of choice because its' low coefficient

of thermal expansion best meets thermal stability requirements. Manufacturing processes, tooling and quality assurance inspection techniques will be developed.

Various telescoping tube deployment actuator concepts will be investigated. One concept will be an inflatable bag that will be folded unpressurized inside the first stage tube during launch. Once on orbit, the bag will be pressurized with dry nitrogen to approximately 10 psi causing the tubes to deploy sequentially. Once fully deployed the inflatable bag will be depressurized. Another concept is a motor driven cable and pulley system. This approach has been developed by industry for other space programs and will be evaluated for this application. A third concept that will be evaluated is a motor driven device which deploys graphite epoxy stems into a Stewart platform configuration.

The structural/mechanical connection between each stage of the 3 telescoping tubes is particularly critical for ensuring the structural stability and alignment of the EOB. Passive latching systems as well as active electro-mechanical concepts will be developed.

8.8 Deployable Booms

Industry has developed several versions of deployable booms that can be compactly stored prior to launch and either passively or actively deployed on orbit. These systems have been successfully flown on many spacecraft programs and will be evaluated for this application.

8.9 Other Concepts

Unmanned deployment of large light-weight rigid structures that can be compactly stored before launch, automatically deployed on orbit, support heavy masses and be structurally and thermally stable to arc second precision tolerances over long periods of time is a new and challenging technology. The HTXS and the Next Generation Space Telescope are two missions that could benefit from such a development program. In parallel with this study, it is recommended that industry be encouraged to propose alternative approaches or concepts.

8.10 Precision Remote Control Alignment Systems

Five arc second magnitude alignment requirements between each of the instrument optical assemblies and their respective detector assemblies may necessitate the incorporation of precision remote controlled electro-mechanical alignment devices. These systems also may be necessary to ensure that possible misalignment caused by the deployment, thermal instability and aging can be corrected.

Various approaches to achieving the required alignment will include precision remote controlled 2-axis gimbal and x-y lateral translational systems. Actuators and position control systems using lasers or LEDs that provide alignment signals will be designed.

8.11 Thermal Control

Thermal stability, operating temperature and temperature gradient requirements are significant constraints that will drive the design of all elements of the EOB. For example, the

cryo-cooler outer shell temperature cannot exceed 120K, the SXT mirrors must be maintained at 15 deg. C and its' radial temperature gradient must not exceed 0.5 deg. C. Also the EOB that provides the ~ 8 meter focal length and the alignment systems that support the instrument components must be thermally stable to preclude 5 arc second magnitude motions throughout the 100 hours observation period.

As a part of the EOB system design various temperature control techniques and approaches will be investigated. These will include both passive (paints, coatings and thermal blankets) and active (heaters and thermostats) systems.

8.12 Deployable signal and power cables

Mechanisms that enable the interconnecting signal and power cables to deploy with the extendible structure will be designed.

8.13 Deployable Scattered Light Shield

The SXT and the CCD detectors are sensitive to scattered light. One method that could minimize scattered light is to completely enshroud the light path between the SXT optics and the detectors with a flexible cloth like shield that deploys along with the extendible structure. Material selection, pre-launch packaging and deployment mechanism designs will be studied. The HXT is not as sensitive to scattered light and therefore requires no shielding.

8.14 Milestones for the EOB Development

Milestones for EOB Development

| Milestones | Date |
|---|--------|
| Instrument interface requirements defined | 6/1/97 |
| Confirm launch vehicle, orbit, ground station assumptions | 6/1/97 |
| EOB-Spacecraft interfaces defined | 6/1/97 |
| Deployable structures concepts evaluated, 2 concepts selected for detail design and analysis | 3/1/98 |
| EOB systems design completed | 9/1/98 |
| Complete evaluation of 2 deployable concepts, 1 selected for hardware development | 1/1/99 |
| Spacecraft design completed | 3/1/99 |
| Precision alignment engineering models completed | 6/1/99 |
| Complete cable and light shield engineering models | 6/1/99 |
| Deployable structure engineering model completed | 3/1/00 |
| All engineering models tested | 9/1/00 |

9 Mission Study

The goal of the HTXS mission study is to complete a preliminary design for an HTXS mission (instrumentation, spacecraft, and operations) that achieves the stated scientific objectives at a minimum of cost and technical risk.

9.1 Study Areas

9.1.1 Science Working Group and Science Study Team

The mission study involves updating and extending the science requirements, for the entire payload. These science requirements will be converted into detailed engineering requirements for the science instruments and spacecraft. The mechanism for refining these requirements will continue to be a series of quarterly meetings of the Science Working Group (SWG) members. The HTXS Science Study Team (SST) consists of about 60 scientists at 15 institutions; the HTXS SWG is a subset of the SST consisting of approximately 20 members, from the same institutions. SWG meetings to date have rotated among several of these institutions, and are open to all members of the HTXS Science Study Team as well as members of the astronomical community at large.

The HTXS SWG and SST members review the on-going design efforts of the various engineering groups, and ensure that these efforts continue to meet the science requirements of the mission. These team members are responsible for integrating the scientific instrumentation into a unified mission approach.

SWG and SST members are also responsible for providing science simulations, both in support of trade studies called out in other sections of this report, and as an aid for determining and refining specific mission parameters. These science simulations are driven by the HTXS team, and incorporate the ideas and priorities of the larger science community as communicated to the HTXS study team via open meetings, www-homepages, and scientific workshops.

9.1.2 Reports

The Mission Study activity also encompasses the generation of reports and presentations to NASA, various advisory committees, and the overall community. These reports are generated on an as-needed basis throughout the study period. In addition to hardcopy versions, these reports will be made available on the World Wide Web via the HTXS homepage.

9.1.3 Technical Interchange Meetings and Contractors Visits

The Mission Study will also support Technical Interchange Meetings (TIMs) between the various members of the study, as well as visits to appropriate contractors and potential contractors.

9.2 Pre Phase-A mission studies

Pre Phase-A studies will be conducted to establish a mission conceptual design that will meet the requirements of the HTXS scientific investigation. The orbit, launch vehicle, spacecraft, instrument interface accommodations, ground stations and operations will be studied. The goal of the study is to provide sufficient detail to evaluate the technical feasibility and cost of implementing the HTXS mission.

Preliminary studies have identified significant technical challenges that will require detail design, analysis and trade off studies. These include systems that will meet the instrument pointing accuracy and long term stability requirements; extendible structures to provide the 8.5 to 12 meter instrument focal lengths; thermal control systems that will ensure distortion free optics, thermal stability and optimized cryocooler design; RF communications systems that will accommodate the large volume of data accumulated by the multiple observatories and be compatible with relatively low cost 11 meter antenna class ground stations. Since the scientific value of the HTXS mission is enhanced by increasing the number of spacecraft in orbit, the design studies will emphasize low cost approaches to components, integration and test, and on orbit operations.